CERN-ACC-2021-0007

November 2021
stephane.fartoukh@cern.ch

LHC Configuration and Operational Scenario for Run 3

S. Fartoukh, S. Kostoglou, M. Solfaroli, G. Arduini, H. Bartosik, C. Bracco, K. Brodzinski, R. Bruce, X. Buffat, M. Calviani, F. Cerutti, I. Efthymiopoulos, B. Goddard, G. Iadarola, N. Karastathis, A. Lechner, E. Métral, N. Mounet, F.-X. Nuiry, S. Papadopoulou, Y. Papaphilippou, B. Petersen, T. Persson, S. Redaelli, G. Rumolo, B. Salvant, G. Sterbini, H. Timko, R. Tomás, J. Wenninger

Keywords: LHC Run 3

Summary

After its second successful run period, the Large Hadron Collider (LHC [1]) shut down for three years with the plan of being recommissioned in 2022 for a three-year physics production period, the Run 3. The future restart of the machine coincides with the completion of the LHC Injectors Upgrade (LIU) project [2], offering to the LHC the opportunity and the challenge to operate with up to two times higher beam brightness, pending the complete installation of the High-Luminosity LHC (HL-LHC [3]), which should take place in Long Shutdown 3 (LS3). In this context, Run 3 is clearly a transition between the LHC and the HL-LHC, with key ingredients which will be made available, either gradually (LIU beam) or immediately (ATS optics [4]). Run 3 shall therefore be exploited not only for performance, but also as a full scale demonstrator of the HL-LHC in terms of beams, optics and beam manipulation (e.g. β^* levelling over a very large dynamic range). To this aim, the so-called LHC configuration, namely the optics, needs to be adapted in order to cope or mitigate constraints of different nature, from beam brightness limitations due to the machine impedance, to specific desiderata of some LHC experiments. After reviewing these constraints, including the intensity limitations coming from the existing hardware, the beam parameters targeted for the LHC in Run 3 are given. A possible solution for the machine configuration will then be described, and analyzed from various perspectives, which should not limit the machine performance over the full Run 3, and should enable to double the integrated luminosity delivered so far to the two high luminosity insertions of the LHC.

1 Beam parameter targeted for Run 3

During the third exploitation period of the LHC, an unprecedented ramp up of the beam intensity will take place in the LHC injector chain, thanks to the completion of the LIU project. The ultimate objective is to meet the HL-LHC beam parameter target towards the end of Y2024, in particular

with bunch trains containing 2.3×10^{11} p/b at SPS extraction (see Sub-section 1.1), to be compared with $1.1 - 1.2 \times 10^{11}$ p/b regularly delivered in Run 2 (and up to 1.35×10^{11} p/b). On the other hand, the LHC will have to wait until Run 4 in order to fully profit from such a beam, due to intensity limitations in several sub-systems of the Ring, which are not planned to be upgraded in Run 3. These limitations are summarized in Sub-section 1.2, which, in the best and worst cases, lead to two possible extreme beam parameter sets at start of stable beam (SB) in Run 3 (see Sub-section 1.3).

1.1 Beam parameters forecast at SPS extraction

Parameters	2022	2023	2024
Bunch population ([10^{11}] p/b)	1.40 → 1.80	1.80 → 2.10	2.10 → 2.30
Norm. transverse emittance ([μm])	1.30	1.30 → 1.55	1.55 → 1.70

Table 1: Beam parameters expected at SPS extraction in Run 3 for BCMS (or 8b4e) proton beams. The intensity ramp up is planned to be conducted at constant transverse emittance during the first year, till reaching the beam brightness limit in the injector towards the end of 2022 (1.8×10^{11} p/b within $\gamma\epsilon = 1.30\,\mu$m). The bunch population limit mentioned in each year will be targeted in dedicated machine studies only. In particular, an operational beam with 1.8×10^{11} p/b will a priori be available for the LHC only as of 2023.

The beam parameters at SPS extraction will drastically change year by year in Run 3. Assuming a BCMS [5] beam structure, possibly combined with a few 8b4e [6] bunch train inserts in order to mitigate the heat-load due to electron cloud (see Sub-section 1.2), the forecast by the LIU project are summarized in Tab. 1 [7]. In 2022, a bunch population of up to 1.8×10^{11} p/b within a transverse normalised emittance of $\gamma\epsilon = 1.30\,\mu$m is planned to be demonstrated in dedicated studies. This beam, however, will only be operational beginning of 2023. Later on, the bunch population will continue to be pushed while operating at the beam brightness limit in the injector, namely up to 2.1×10^{11} p/b (within $\gamma\epsilon = 1.55\,\mu$m) at the end of 2023, and meeting the HL-LHC target of 2.3×10^{11} p/b (within $\gamma\epsilon = 1.70\,\mu$m) at the end of 2024.
To be noted that in view of the post-LS2 difficulties, the original target of re-establishing the pre-LS2 performance has not yet been reached and may not be achieved by the end of 2021. In addition, a lot of the planned beam performance study and ramp-up time has been lost or used for continuing equipment commissioning, meaning that some commissioning will still remain to be done in 2022. An exchange of one MKDV kicker during the 2021/22 YETS is planned to overcome one specific and important limitation, which will then open the door to the studies and performance stabilization with higher intensities. The subsequent 2022 performance ramp up will probably be slower than was originally planned, given the technical problems, lessons learned and delays encountered in 2021. However, the basic functionalities of the upgraded systems have, in general, been demonstrated and there are good indications that the SPS will be able to deliver 1.4e11 p/b for LHC in the course of 2022, depending on the progress with new equipment conditioning and recommissioning.

1.2 Intensity limitations in the LHC

1.2.1 Injection System

The injected beam passes through 5 horizontally deflecting steel septum magnets (MSI) and four vertically deflecting kickers (MKIs) [1]. The power dissipated in the MKI ferrites depends on the beam parameters (total intensity and bunch length), on the magnet beam coupling impedance, and on the available cooling mechanisms. After the MKI-8D replacement in YETS17-18, the next limiting magnet (MKI-8C) is expected to restrict the bunch intensity to 1.45×10^{11} p/b for a bunch length of 1.1 ns and 2592 bunches, assuming Gaussian bunch profiles [8]. With the MKI-8C replacement by an upgraded kicker, which was initially foreseen in LS2 but is now postponed to the YETS22-23, further studies with 2808 equidistant bunches show that the above restriction can be relaxed up to 1.80×10^{11} p/b in *permanent regime*, provided that the bunch length is pushed to 1.35 ns [8]. Assuming a somewhat reduced bunch length, this means that in *transient regime* a bunch population of 1.80×10^{11} p/b could still, in principle, be sustained without exceeding the MKI temperature limit, but for a few hours, depending upon the temperature of the ferrite yoke at the start of the fill. Accordingly, the bunch length has been chosen to 1.2 ns (i.e. 9.0 cm r.m.s.) for the entire Run 3, compared to 1.0 ns in Run 2, but might need to be adjusted depending on the needs and observations in Run 3, in particular in 2023 and 2024, when this parameter could become critical from the MKI heating perspective. To be noted that the complete MKI upgrade (in particular in Pt2) is foreseen to be deployed in LS3 in order to make the injection system fully compatible with the HL-LHC beam intensity target (2.30×10^{11} p/b).

1.2.2 Collimation system

The LHC collimation system provides an efficient cleaning of the beam halo during the full LHC cycle. A major upgrade of the system is foreseen in LS2 and LS3 in order to significantly decrease the contribution of the collimators to the transverse impedance of the ring. The collimation settings in Run 3 are planned to be similar to those used in 2017/2018 [9] in order to optimize the β^* reach. There is no particular concern related to the IR3/IR7 collimator robustness for bunch intensities of 1.8×10^{11} ppb or above [10].

1.2.3 Beam dump System

The LHC beam dump system (LBDS) of each ring consists of 15 extraction kicker magnets (MKD), 15 steel septum magnets (MSD) and 10 modules of dilution kicker magnets (MKB) [1]. While no issues have been identified for the extraction kickers, installing two additional modules to the MKB system will increase the margins in case of failure [11]. The most critical components of the LBDS, affected by the increased intensity, are the main dump (TDE assembly and its upstream and downstream windows), and the septum and main ring protection devices, TCDS and TCDQ, respectively. Except for the upstream window of the TDE, all the intensity limitations summarized below are rather independent of the beam emittance.

TDE

The LHC Beam Dump (TDE - Target Dump External), is conceived to absorb safely each of the two circulating beams. The core is composed of a stack of low- and high-density graphite segments

in order to appropriately dilute the impinging proton beam, and contain the adiabatic temperature rise due to the energy deposition. The material is contained in a 12 mm thick duplex stainless steel (318LN) vessel. The graphite sector is contained in gaseous nitrogen to create an inert atmosphere and thus avoid graphite oxidation, that may lead to mass loss. FLUKA simulations indicated that for a bunch population of 1.8×10^{11} p/b, the temperature increase of the TDE core following a beam dump ranges in between 1500°C and 2400°C, for regular and non-regular dumps, respectively [12].
During the course of LHC Run 2, the dump block and the adjacent connection line suffered from different nitrogen leaks because of damaged gaskets and loose flanges. The damage could be attributed to the violent vibrations induced by the shock heating of the TDE vessel during the beam dumps. During LS2, the dump support system, beam windows and related infrastructure were upgraded to ensure compatibility with a bunch population of 1.8×10^{11} p/b during Run 3 [13]. In particular, both upstream and downstream dump windows are now made of fully forged Ti Grade 5, since the previously used grade (Ti Grade 2), would not have been compatible with this bunch intensity [14].
The vacuum window at the end of the extraction line, about 10 m upstream the TDE, will also be upgraded in a similar fashion and installed during YETS 2021-22, employing Ti Grade 5.
Larger uncertainties exist for the behavior of the low-density graphite, for which the temperature is not the only critical factor. A large effort of characterization and modelling is ongoing with NTNU (*Norges teknisk-naturvitenskapelige universitet*) in Norway, in order to be able to understand its behavior. In particular, following the results of a parasitic irradiation during the HRMT43 experiment in HiRadMat conducted at the end of 2018 [15], doubts exist on the integrity of the low-density graphite sector (composed of SGL Sigraflex sheets). The robustness of the TDE core material will be probed in more realistic configurations via a dedicated beam impact experiment in the HiRadMat facility in 2021, with results to be expected in early 2022.
Moreover, a complex autopsy of at least one of the two radioactive dumps used during Run 1 and Run 2 will be performed early 2022, following the observation of cracked extruded graphite disks holding the Sigraflex sector in place. This will provide essential information on the response of the entire dump system to beam impact.
These investigations will confirm if the graphite core can sustain beam operation with 1.8×10^{11} p/b in Run 3.

TCDS

The two existing TCDS absorber modules are not expected to be a limitation for Run 3, as they were designed for a bunch population up to 1.7×10^{11} p/b (with a maximum of 40 consecutive bunches possibly hitting the TCDS in case of asynchronous dump). The original design studies for 1.7×10^{11} p/b showed that the Ti-6Al-4V blocks at the end of the second TCDS module may be subject to plastic deformation, but this was considered acceptable [16]. New simulation studies suggest that the plastic strain reaches 1.2% in the titanium-alloy block in case of HL-LHC bunch intensities (2.3×10^{11} p/b) [17]. Although the material can still elongate before reaching the necking point ($\sim$10%), the material integrity cannot be guaranteed for several accidental shots at this intensity. It is nevertheless expected that the induced distortion of the titanium-alloy block remains acceptable in case of asynchronous beam dumps with 1.8×10^{11} p/b in Run 3.
Another set of simulations was also recently conducted to study the other TCDS blocks, made

of carbon-reinforced-carbon (CC) and graphite [18]. The studies were based on updated material properties, which were obtained in a new material characterization campaign. The results indicate that the CC and graphite blocks of the TCDS can also sustain the impact of bunches with 1.8×10^{11} p/b in Run 3.
In all cases, a series of checks and measurements, with and without beam, has been defined to assess the integrity of both the TCDS and TCDQ (see next paragraph), before restarting operation after the occurrence of an asynchronous beam dump [19]. Moreover, an endoscopic inspection might be possible during the following YETS to evaluate the actual status of the critical absorbing blocks.

TCDQ

The TCDQ absorber was already upgraded in LS1 considering the HL-LHC beam parameters, for which the power deposition in case of asynchronous dump was well within the material limits. However, during Run 2, new MKD erratic failure scenarios (Type-2) have been observed, during which the particle density hitting the TCDQ could be higher than expected, thus limiting the minimum possible TCDQ half-gap. Considering this new failure mode, thermo-mechanical simulations with a TCDQ half-gap of 2.5 mm revealed that an intensity of 1.7×10^{11} p/b is reachable with a good safety factor margin [20], whereas permanent damage may occur in the most loaded CC block at HL-LHC bunch intensities (2.3×10^{11} p/b) [18]. The damage is, however, expected to be very localized along a small strip close to the block surface. Based on these results, it is estimated that the TCDQ blocks can sustain the impact of bunches with 1.8×10^{11} p if the TCDQ is located at a distance of 2.5 mm from the beam. An experimental confirmation of the block robustness will be obtained in the HiRadMat test in 2021.
The TCDQ opening is expected to be 3.57 mm in Run 3 for both beams, considering a normalised gap of $7.3\,\sigma$ as in Run 2 [9], a reference emittance of $\gamma\epsilon = 3.5\,\mu$m, 7 TeV for the beam energy, and a horizontal β-function of about 510 m at the TCDQ which will be kept constant during the full cycle (see Section 3). Therefore, by comparing with the above-mentioned minimum gap of 2.5 mm, this setting should leave a sufficient margin of 1.1 mm, for alignment errors (usually taken as ± 0.30 mm [21]) and the interlock threshold before dump for the BPM at Point 6 (set to $1.5\,\sigma$, i.e. 0.73 mm, in Run 2).

1.2.4 RF System

The injected beam is captured, accelerated and stored using the 400 MHz superconducting cavity system [1]. The klystrons are rated to deliver 300 kW of RF power, but in operation the observed readings reveal a saturation at 250-280 kW, although with large error-bars. In Run 2, several machine development studies [22] have been performed in order to identify the optimal settings, both to improve the SPS-LHC matching and to reduce the power consumption for the LIU beams. A beam with bunch intensity of 1.8×10^{11} p/b can be injected in the LHC by setting the RF voltage at 6.4 MV, while guaranteeing a good RF capture in the LHC using the SPS Q20 optics [23]. On the other hand, as soon as the LHC ring is completely filled, in particular during the ramp and at flat top energy, it is important to recall that the RF power consumption can be made independent of the beam current thanks to the full-detuning beam-loading compensation scheme.
At the targeted energy of 7 TeV, the present system is fully able to operate at the required 16 MV

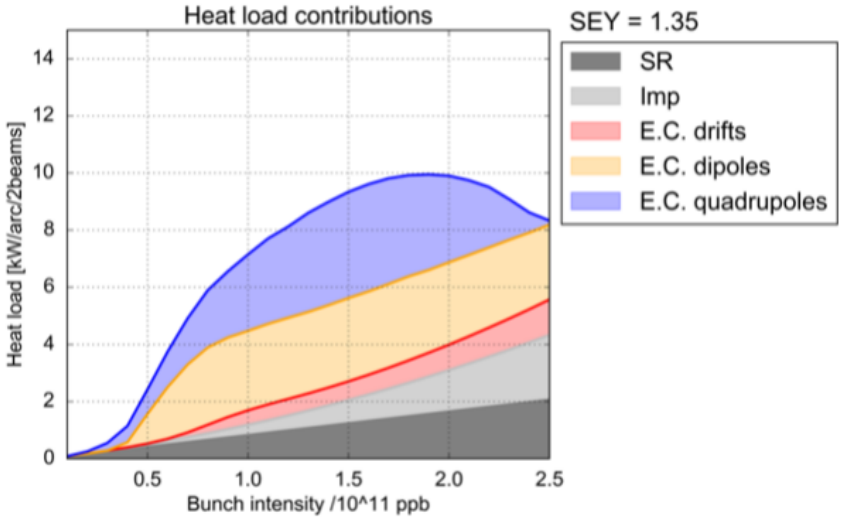

Figure 1: Various contributions to beam induced heating in the LHC arcs as a function of the bunch population: synchrotron radiation at 7 TeV (SR), impedance (Imp) and electron cloud (E.C.) for an SEY of 1.35 (as estimated in average for the high load sectors), assuming BCMS beams (packed into trains of 48 bunches spaced by 25 ns). The cryo-cooling capacity limit of $\approx$ 10 kW/arc is expected to be reached for a bunch population of 1.8×10^{11} p/b.

for 1.2 ns long bunches, as targeted to ease the controlled emittance blow-up in the ramp. Even slightly longer bunches targeted at the end of ramp (EoR), e.g. to mitigate the MKI heating, would be acceptable for the RF system.

1.2.5 Heat-load and cryo-cooling capacity

The LHC superconducting magnet coils (arcs, dispersion suppressors and inner triplets) are immersed in a bath of superfluid helium at a pressure of about 0.13 MPa and a maximum temperature of 1.9 K [1].

LHC arcs

As far as the heat-load due to e-cloud is concerned, the LHC sectors can be categorized into high load sectors (S78, S81, S12, S23, especially S12 and S23) and low load sectors (S34, S45, S56, S67) where the average Secondary Electron Yield (SEY) parameter is estimated to be 1.35 and 1.25, respectively. Fig. 1 shows the various contributions to heat-load for a high load sector assuming a BCMS beam structure. In particular, a bunch population of 1.8×10^{11} p/b corresponds to a worst case in terms of beam induced heating in the arcs, but it is still compatible with the cryo-cooling capacity limit of $\approx$ 10 kW/arc in the high load sectors (i.e. $\approx$ 200 W/half-cell [24]). Considering instead a standard 25 ns filling pattern (with trains of 72 consecutive bunches), this limit would be exceeded by 10 %, which clearly favours the BCMS beam structure for Run 3, along with the considerably smaller injected emittance for BCMS bunch trains (which should maximize the beam transition to flat top energy), and at a cost of only a marginal reduction in terms of total number of bunches (see Fig. 2). Operating the machine at the cryo-cooling capacity limit, a backup

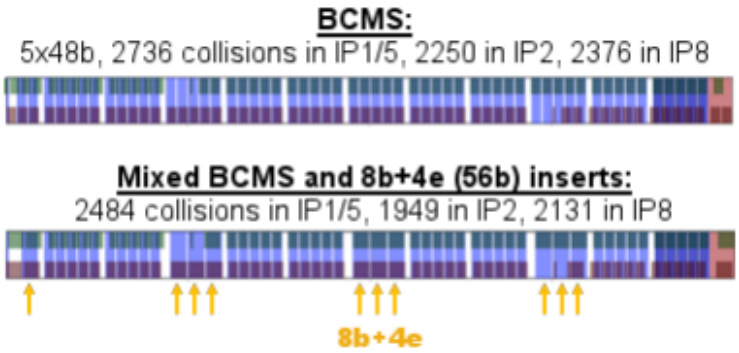

Figure 2: Possible filling schemes considered for the LHC operation in Run 3. The first one is a pure BCMS beam, resulting in 2736 collisions in the two high luminosity experiments. The second one is a hybrid filling scheme, consisting of a BCMS beam structure mixed with 8b-4e inserts, in order to restore margin in the cryo-cooling capacity of the LHC arcs by mitigating the electron cloud induced heat-load. A margin as large as 2.5 kW/arc (i.e. 25 %) results into a ~ 10 % reduction of the total number of bunches, corresponding to 2484 collisions at IP1/5 and 1949/2131 at IP2/8 (vs. 2736 and 2250/2376, respectively, for a pure BCMS scheme).

filling scheme shall however already be considered at this stage. As an extreme example, in case of unforeseen limitation by 25 % of the cryo-cooling capacity of the arcs after LS2 (i.e. 7.5 kW/arc instead of 10 kW/arc), or, said differently, in case of an increase of the beam induced heating by 33 % w.r.t. pre-LS2 observations and extrapolations, a backup solution would consist of a hybrid scheme [25] with 8b4e bunch trains inserted into the BCMS filling pattern, reducing the number of collisions by about 10 % in ATLAS, CMS and LHCb (see Fig. 2).

Inner triplets

The cryo-cooling capacity of the inner triplets in IR1 and IR5 for dynamic heat-load compensation was measured at 270 W (306 W for the total heat-load). Within this capacity, a maximum luminosity of $2.2 \times 10^{34}\,\mathrm{cm}^{-2}\mathrm{s}^{-1}$ at 6.5 TeV, or about $2.0 \times 10^{34}\,\mathrm{cm}^{-2}\mathrm{s}^{-1}$ at 7 TeV can be maintained [24]. In case of luminosity leveling, the impact of operating the inner triplets at the cryogenics limit is marginal (2 %) on the cooling capacity of the beam screens in the adjacent arcs. To be noted that a peak luminosity of $2.0 \times 10^{34}\,\mathrm{cm}^{-2}\mathrm{s}^{-1}$ corresponds to $\langle\mu\rangle \approx 52$ pile up (PU) events per bunch crossing for a pure BCMS filling scheme with 2736 collisions at IP1 and IP5, and to $\langle\mu\rangle \approx 57$ for the backup hybrid scheme with about 9 % less collisions shown in Fig. 2. Therefore, in both cases, the PU limit of 60 recommended by the experiments (see e.g. [26]) remains in the shadow of the cryo-cooling capacity limit of the inner triplets.

1.3 Beam parameter range targeted in Run 3

Combining all the above concerns, together with the expected intensity ramp up of the LIU beam, a challenging but still realistic intensity target for operating the LHC in Run 3 is a bunch population of 1.4×10^{11} p/b in 2022, pushed to a maximum of 1.8×10^{11} p/b in 2023/2024, within an injected

emittance of 1.3 μm (for BCMS beams). Due to intra-beam scattering (IBS) effects, this emittance should rise up to 1.65 μm after 40 minutes spent on the injection plateau before the start of the ramp (see Fig. 3). Considering an emittance growth budget in between 10 % and 50 % in the ramp, the transverse emittance at start of SB should then range in between 1.8 μm and 2.5 μm. To be noted that an overall emittance growth budget of 50 % is still compatible with the unexplained emittance extra blow-up observed during the ramp (but also at injection) in Run 2 [27].

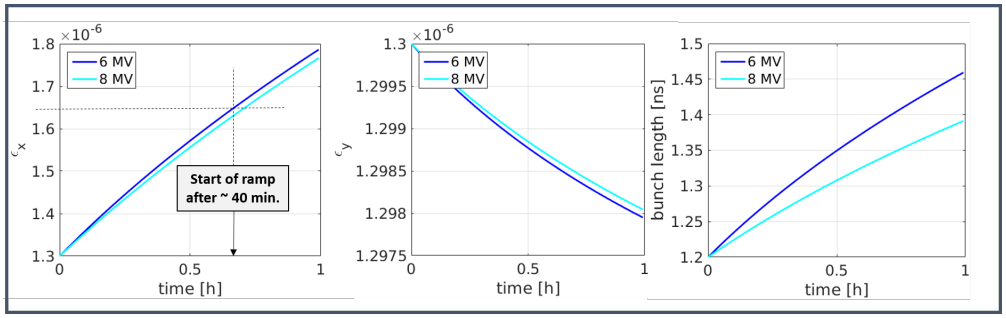

Figure 3: Transverse and longitudinal emittance growth due to IBS on the injection plateau at 450 GeV, assuming a bunch population of 1.8×10^{11} p/b, an injected transverse emittance of 1.3 μm, and a bunch length of 1.2 ns, for two possible settings of the RF voltage.

Finally, based on the above discussion on possible cryo-cooling limitations in Run 3, the total number of bunches should range in between 2736 (+12 non-colliding) bunches in 2022, possibly down to 2484 (+12) bunches in case of heat-load limitation at high intensity in 2023 and 2024. This range of beam parameters is summarized in Tab. 2, at start of SB, assuming no beam transmission loss from injection to flat top energy.

Calendar Year	2022	2023 / 2024
Number of bunches	2748	2748 $\rightarrow$ 2496
Number of collisions at IP1/5	2736	2736 $\rightarrow$ 2484
Number of collisions at IP2	2250	2250 $\rightarrow$ 1949
Number of collisions at IP8	2376	2376 $\rightarrow$ 2131
Bunch population ([10^{11}] p/b)	1.40	1.80
Bunch length ([ns])	1.20	1.20 ($\rightarrow$ 1.35)
Norm. transverse emittance ([μm])	1.80 $\rightarrow$ 2.50	

Table 2: Beam parameter range at start of SB in Run 3, taking into account the LIU beam intensity ramp up and various limitations in the LHC. The uncertainty on the number of bunches in 2023/2024 should be clarified in 2022 based on heat-load measurements. The uncertainty on the beam emittance at start of SB depends on the emittance control in the ramp which will be demonstrated in Run 3. Finally, a small uncertainty still exists on the minimum achievable bunch length at flat top energy depending on the MKI heating control at high intensity.

Unless specified differently, the best beam parameters will be assumed in all the rest of the paper, namely a bunch population of 1.4×10^{11} ppb and 1.8×10^{11} ppb in 2022 and 2023/2024, respectively, within a transverse emittance of 1.8 μm and a r.m.s. bunch length of 9 cm (1.2 ns)

at start of SB, with 2736, 2376 and 2250 collisions per turn at IP1/5, IP8 and IP2, respectively. For performance estimate (see Section 2), the recently confirmed beam energy of 6.8 TeV will be assumed, while a beam energy of 7.0 TeV has been used for the tracking studies reported in Section 3.

2 LHC experiment Desiderata versus machine constraints

2.1 ATLAS and CMS

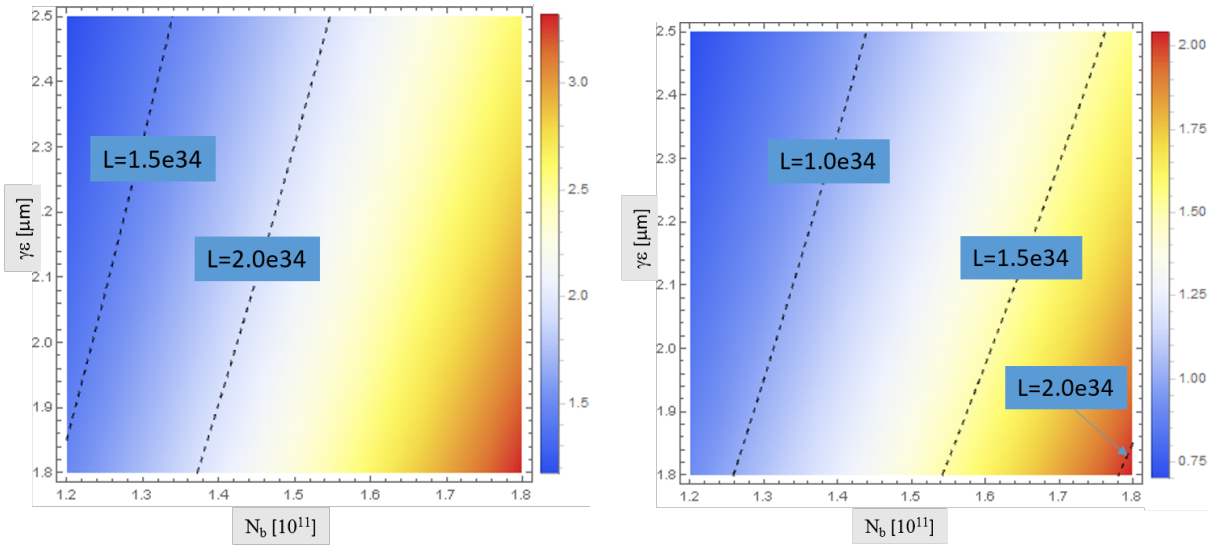

$\beta^* = 60$ cm $\beta^* = 1.2$ m

Figure 4: Peak luminosity in ATLAS and CMS as a function of the bunch population and transverse emittance for two different values of β^*, taking an half-crossing angle of $\Theta_c/2 = 160\mu$rad in both cases. 2736 collisions per turn are assumed at IP1 and IP5 at a c.m. energy of $2 \times 6.8 = 13.6$ TeV. The r.m.s bunch length is set to 9 cm.

The main constraints from the ATLAS and CMS experiments lie in the fact that the number of pile up events per bunch crossing should be less than 60 [26], within a luminous region in between 32 mm r.m.s. (as in Run 2) and ~ 50 mm, above which the inner tracker could be blind to a small fraction (percent level) of the vertices [28].
Regardless of the number of collisions at IP1 and IP5 in the two extreme cases considered so far (namely 2484 or 2736, see Tab. 2), and as already discussed, the PU constraint is automatically fulfilled with a luminosity levelled to $2 \times 10^{34}\,\mathrm{cm}^{-2}\,\mathrm{s}^{-1}$. Concerning an appropriate choice of the optics parameters at start of SB (and the resulting luminous region), Fig. 4 shows a color plot of the peak luminosity as a function of the bunch population and of the transverse emittance, for two different values of β^* (namely 60 cm and 1.2 m), assuming in both cases a beam energy of 6.8 TeV and 2736 collisions at IP1 and IP5, with a half-crossing angle of 160 μrad as in 2018. Considering the beam intensity projection for 2022 (1.4×10^{11} p/b) and 2023/2024 (1.8×10^{11} p/b), and assuming a good emittance preservation in the ramp ($\gamma\epsilon \sim 1.8\,\mu$m at flat-top energy), it is rather clear that the choice of β^* at start of luminosity levelling (SoL) has to be modified in between

the first year of Run 3 and the rest of the run. $\beta^* = 60$ cm seems to be an appropriate choice for the 2022 run, while an initial β^* as large as 1.2 m could be needed in 2023/2024 assuming that a good emittance control in the ramp would have been demonstrated in 2022.
The choice of crossing angle at start of SB for 2022 is a compromise between an as small as possible β^*-levelling range for the first year of Run 3 (only a factor of 2 from 60 cm down to 30 cm), and a further reduction of the Piwinski angle, namely $\phi_w \propto \Theta_c \sigma_z / \sqrt{\beta^*}$, with respect to the 2018 run ($\beta^* = 30$ cm with $\Theta_c/2 = 160\,\mu$rad and $\sigma_z = 7.5$ cm [29]), in order to minimise the risk of beam instabilities when the two beams are put in collision [30]. Even for a bunch population of 1.8×10^{11} p/b at start of levelling in 2023/2024, a half-crossing angle as large as to $160\,\mu$rad is over-sized in order to mitigate the long-range beam-beam (BBLR) interactions at $\beta^* = 1.2$ m. Such a crossing angle remains however preferable, again to minimise the β^* dynamic range in stable beam (a factor of 4 from 1.2 m down to 30 cm in 2023/2024), and might be appropriate in order to avoid extra-losses during the first hour of SB, as observed in Run 2 [31]. Then, later on in stable beam, operating at the so-called BBLR limit, i.e. at the minimum possible crossing angle allowed by the BBLR interactions, becomes an interesting option for two main reasons of completely different nature, namely: (i) mitigate the radiation dose taken by the inner triplet, and (ii) optimize the physics conditions for the PPS forward physics experiment [32] in IR5 (H crossing), where the dispersion is maximized at the roman pot locations when the horizontal crossing angle is minimized.
The so-called BBLR limit is a function of β^*, depending on the beam parameters (bunch charge and emittance), and on the actual levelled luminosity in ATLAS and CMS (so as well on the total number of bunches). In practice, it is estimated numerically by tracking for the initial and final β^*, with the initial and final beam parameters, imposing a typical target of $6\,\sigma$ for the dynamic aperture (DA) at start of levelling (high intensity), then in the range of $5.0 - 5.5\,\sigma$ at the end of levelling ("low" intensity, as at start of SB in Run 2), and including the contribution of the other LHC experiments to beam-beam effects such as LHCb, which will run at higher luminosity in Run 3 (see Sub-section 2.4). The normalised crossing angle, obtained this way at the start and end of β^*-levelling, is then interpolated linearly as a function of the bunch population for intermediate β^*. Plugging this linear function into the luminosity formula, and working at a given prescribed levelled luminosity, the bunch population can be extracted as a function of β^* and, finally, the requested parametric variations of the physical crossing angle with β^* can be obtained. This parametric function is shown in Fig. 5, considering the worst case beam parameters of Tab. 2, namely only 2484 collisions at IP1 and IP5, and a poor emittance preservation in the ramp (i.e. $\gamma\epsilon = 2.5\,\mu$m at start of SB, assumed to stay constant in this case). At the prescribed levelled luminosity of $2 \times 10^{34}\,\text{cm}^{-2}\text{s}^{-1}$, the BBLR limit at start of β^*-levelling corresponds to a half crossing angle of $\theta_c/2 = 145\,\mu$rad and $135\,\mu$rad, in 2022 (with $N = 1.4 \times 10^{11}$ p/b and $\beta^* = 60$ cm) and 2023/2024 (with $N = 1.8 \times 10^{11}$ p/b and $\beta^* = 1.2$ m), respectively, and to $\theta_c/2 = 160\,\mu$rad at the end of the levelling (with $N \sim 1.2 \times 10^{11}$ p/b and $\beta^* = 30$ cm, which typically corresponds to the optics and beam parameters in 2018 at start of SB).
The luminosity levelling beam process will therefore contain two well distinct periods, namely:

- a first luminosity levelling period, rather short, acting on the crossing angle at constant β^* till reaching the BBLR limit,
- and a second period of β^*-levelling with concomitant variations of the crossing angle following the BBLR limit.

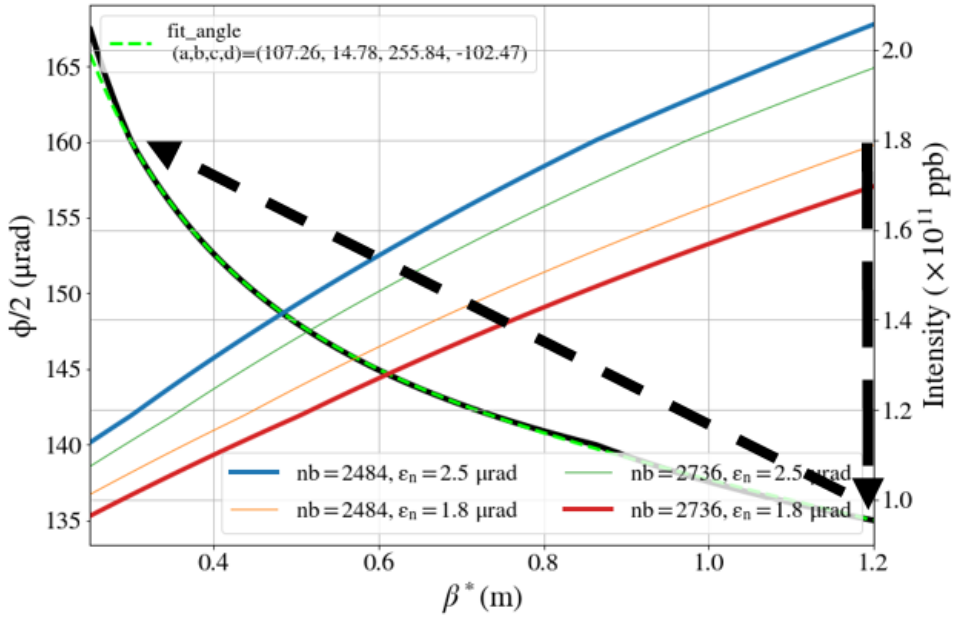

Figure 5: Parametric variations of the crossing angle with β^* in Run 3 calculated for the worst case beam parameters (namely with 2484 collisions at IP1 and IP5 and a poor emittance conservation in the ramp leading to $\gamma\epsilon = 2.5\,\mu$m from start to end of stable beam). Fixing this crossing angle function as input, the evolution of the bunch population is shown during β^*-levelling at the prescribed levelled luminosity of 2×10^{34} cm^{-2}s^{-1}, for the 4 possible beam parameter sets considered in Tab 2.

At the start of the second period, the gain in dispersion at the PPS Roman Pots is expected to be around 15 % in 2023/2024 ($\Theta_c/2 = 135\,\mu$rad instead of $160\,\mu$rad), leading to an improvement in the same proportion for the minimum mass detection threshold. Operating the machine at the BBLR limit should also mitigate by at least 3-4 % (0.5 MGy) the integrated radiation dose which will be taken by the triplet over the whole Run 3 [33], w.r.t. to a scenario where the luminosity would be delivered at a strictly constant crossing angle of $\Theta_c/2 = 160\,\mu$rad.
Beam-beam simulation studies (dynamic aperture) have been performed in order to successfully validate this running scenario, and will be reported in Section 3. For a typical fill of 2022 ($N = 1.4 \times 10^{11}$ p/b) and 2023/2024 ($N = 1.8 \times 10^{11}$ p/b), the profiles of the various quantities (β^*, half-crossing angle, bunch length, bunch charge, emittance and luminosity at IP1 and IP5) are plotted in Fig. 6, together with the evolution of the transverse and longitudinal luminous regions, assuming 2736 collisions and a good emittance preservation in the ramp (i.e. $\gamma\epsilon = 1.8\,\mu$m at flat-top energy). The emittance and bunch length variations in SB have been simulated considering IBS and synchrotron radiation (SR) effects at 6.8 TeV, and considering an additional empirical transverse emittance growth rate of $0.05\,\mu$m/h and $0.1\,\mu$m/h in the horizontal and vertical planes, respectively, as observed in Run 2 [31]. After ~ 15 h of stable beam, the bunch length is assumed to be levelled to 7.5 cm r.m.s. thanks to active RF heating. If really needed, solutions can be found to cure the small excursion above 50 mm which can be observed in Fig. 6 for the longitudinal luminous region in 2023/2024 (e.g. by playing one or a few β^*-levelling steps at constant crossing

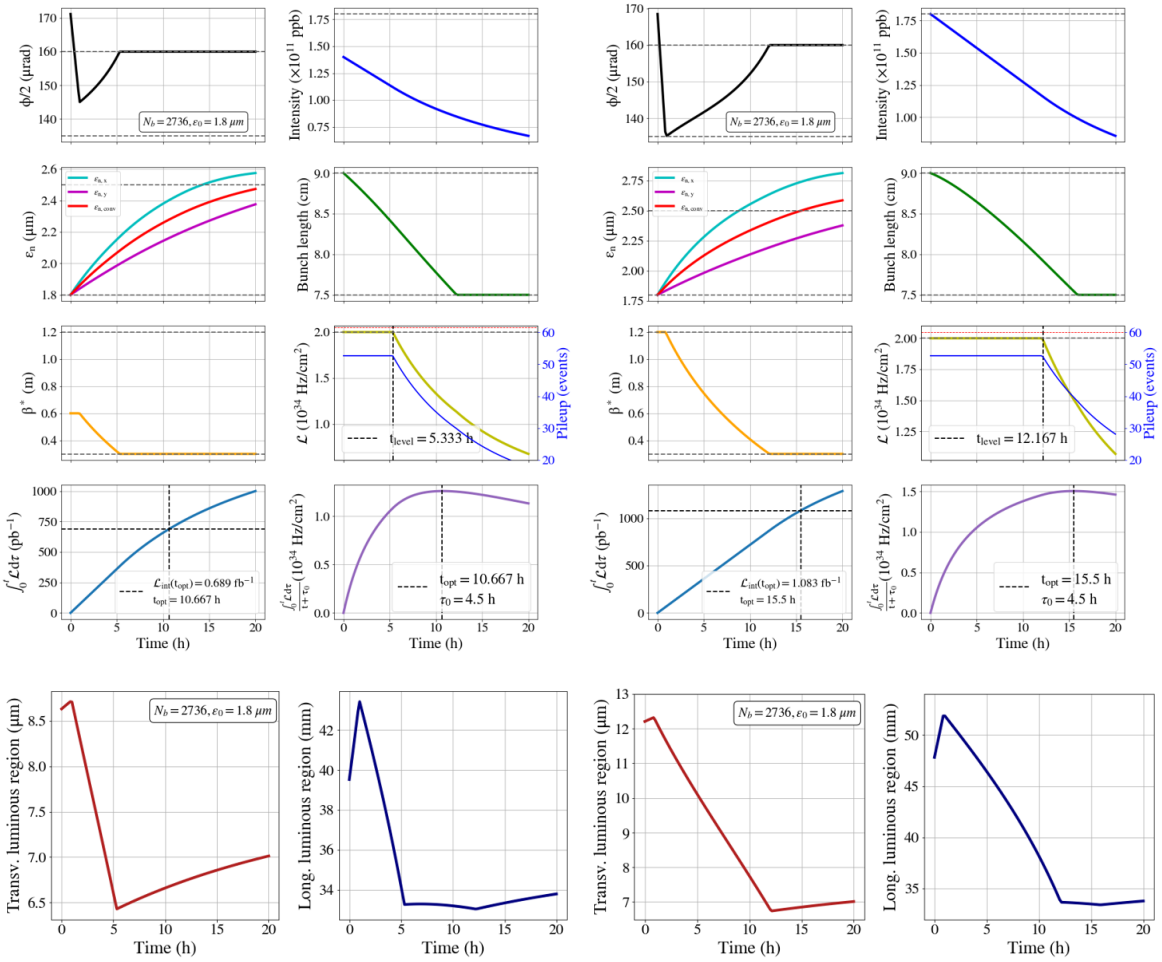

Figure 6: Typical variations of beam and optics parameters in stable beam at 6.8 TeV for 2022 and 2023/2024, together with luminosity, pile-up and integrated luminosity profiles, and evolution of the transverse and longitudinal luminous regions (bottom pictures). Finite β^* steps are neglected in these plots. The luminosity levelling is assumed to be conducted based on the ATLAS peak luminosity which is more penalized than CMS (H crossing) by the horizontal emittance growth due to IBS. The evolution of the longitudinal luminous region contains 4 distinct parts, related to the variations of the loss factor first from the crossing angle at constant β^*, then from the β^*-levelling proper, then from the bunch length shrinkage (from SR) at constant optics, and finally from the transverse emittance growth at constant optics and constant bunch length.

Calendar Year	2022	2023 / 2024			
Machine efficiency	25 %	50 %			
Bunch population $[10^{11}]$ at FT	1.4	1.8			
Collisions at IP1 and IP5	2736	2736		2484	
Norm. emittance at FT $[\mu m]$	1.8	1.8	2.5	1.8	2.5
Levelling time [h]	5.3	12.1	11.4	10.2	9.3
Optimal fill length [h]	10.7	15.5	15.0	13.7	13.3
Integrated luminosity/year $[\text{fb}^{-1}]$	35.4	84.4	83.6	81.2	80.1

Table 3: Performance estimate at 6.8 TeV for 2022 and 2023/2024, considering various possible beam parameters in 2023/2024, assuming a turn around time of 4.5 h, 130 days of pp run per year, and an effective cross-section of 100 mb. The impact of the finite β^* steps during β^*-levelling is neglected, degrading at the percent level or less the performance of each year (e.g. corresponding to a reduction of the 2022 and 2023/2024 performance by $0.3 - 0.4\,\text{fb}^{-1}$ and $1.1 - 1.2\,\text{fb}^{-1}$, respectively, assuming a β^* step of the order of 5 %, see [34] for more details).

angle, before reducing it down to the BBLR limit).
The performance forecast per year is reported accordingly in Tab. 3, for the various beam parameter cases of Tab. 2, assuming 130 days of pp physics per year, a turn around time of 4.5 h, a machine efficiency of 25 % and 50 % for 2022 and 2023/2024, respectively, and an effective cross-section of $\sigma_{\text{eff}} = 100$ mb (for proton burn-off calculation). As shown in Tab. 3, the integrated luminosity delivered in Run 3 will possibly reach, and could even slightly exceed $200\,\text{fb}^{-1}$, in addition to the $190\,\text{fb}^{-1}$ integrated so far by each of the two ATLAS and CMS experiments (Run 1+2). The total ($\sim 400\,\text{fb}^{-1}$) is sensibly beyond the target initially fixed to $300\,\text{fb}^{-1}$ before triplet exchange, and corresponding to an estimate of the triplet damage dose limit of 30 MGy. In practice, however, this dose is deposited at specific locations and azimuthal angles in the coils of the inner triplet, namely (see Fig. 7):

- at the entry of Q2A in IR1 with vertical crossing, and at an azimuthal angle 90 or 270 degrees depending on the polarity of the crossing angle,
- and at the exit of Q2B in IR5 with horizontal crossing, inwards in all cases, since the sign of the crossing angle is fixed by the ring geometry in IR5 (always positive for beam 1 going from the inner to the outer channel when passing IR5, but with the debris already moved to the opposite side at the level of Q2B).

The hottest spot is Q2A in IR1 with vertical crossing coming from the fact that, in pp collisions, a larger fraction of the debris are positively charged (e.g. π^+), and Q1 is always vertically defocusing for the out-going beam in IR1 and IR5. De facto, a year by year polarity reversal of the vertical crossing angle in IR1 becomes a vital ingredient for Run 3, as already proposed and implemented in Run 2 [35]. The present situation and proposal for Run 3 is summarized in Tab. 4. Restarting the machine in 2022 with a negative crossing angle for ATLAS (Beam 1), and choosing two different polarities for operating the machine in 2023 and 2024 (i.e. "$\pm$" or "$\mp$" depending on some possible preferences for 2023 and 2024 coming from the forward physics experiments hosted in IR1) will maximize the triplet lifetime in IR1. In this scenario, the peak doses deposited in the triplets of ATLAS and CMS become very similar [33], estimated to 23 MGy and 24 MGy in the Q2A of IR1

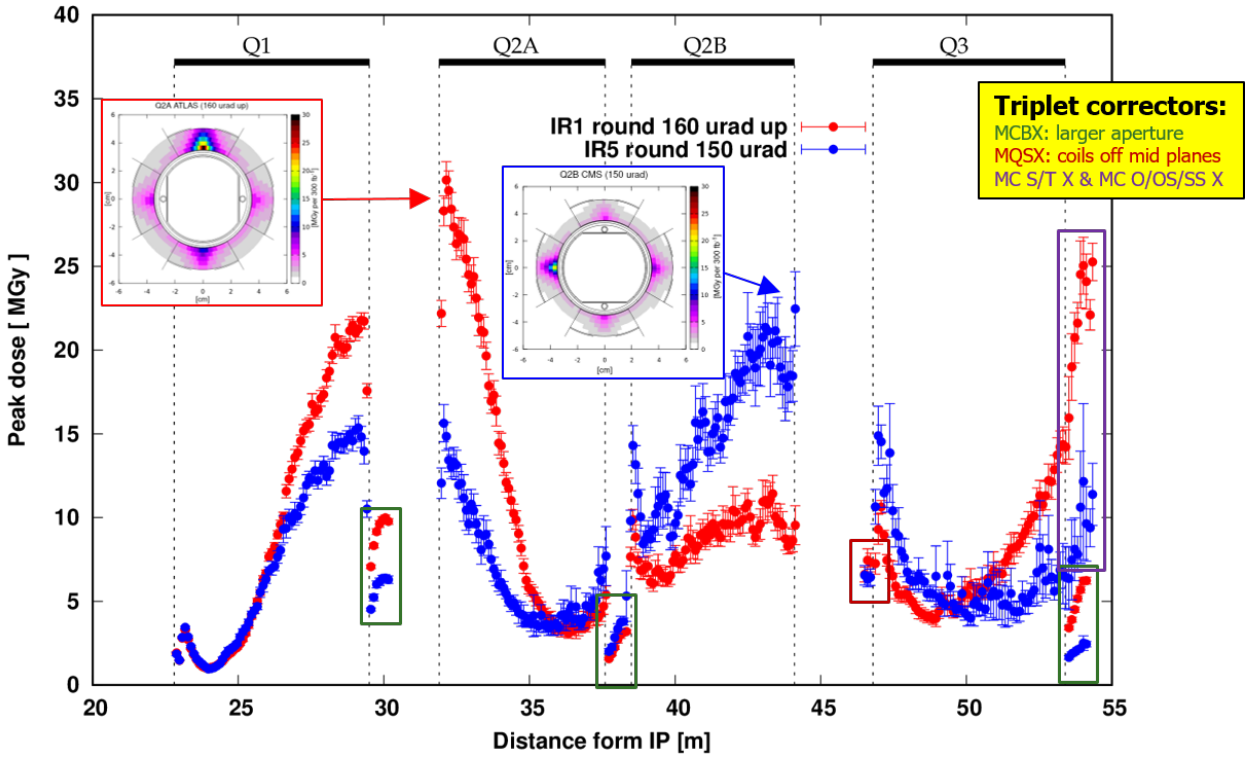

Figure 7: Peak dose deposited in the inner coils of the triplet in IR1 (vertical crossing) and IR5 (horizontal crossing) after 300 fb^{-1}. The most critical magnet is Q2A in IR1 where the peak dose reaches 30 MGy, deposited upwards or downwards depending of the polarity of the crossing angle. These simulations were done for a beam energy of 7.0 TeV.

and Q2B of IR5 (at 6.8 TeV), respectively, after a total of $\sim$ 400 fb^{-1} which should have been integrated at the end of Run 3.

Integrated luminosity[fb^{-1}]	Run 1 + 2	2022 (-)	2023 (-)	2024 (+)	Total
Crossing angle up	115	0	0	85	200
Crossing angle down	75	35	85	0	195
Total	190	35	85	85	395

Table 4: Integrated performance and crossing angle polarity gymnastics in ATLAS to mitigate the peak dose deposited in the inner triplet after $\sim$ 400 fb^{-1}.

2.2 Forward physics experiments AFP and PPS

As in Run 2, the forward physics (FP) experiments AFP [36] and PPS [32] (hosted in IR1 and IR5, respectively) will keep running smoothly in parallel with the ATLAS and CMS physics data taking. These two FP experiments rely on Roman Pots (RP) installed in the matching section, essentially in between Q5 and Q6. With the large dynamic β^*-range expected in Run 3 (a factor of 2 in 2022, and up to 4 in 2023/2024), the transport matrix from the IP to the RP's would however

change drastically in stable beam if standard optics squeezing techniques were used to vary β^*, i.e. by acting on the IR1 and IR5 matching quadrupole settings, which would add a substantial level of complexity for the detector calibration of these two FP experiments. This complexity can however be overcome if the β^*-levelling beam process is performed in telescopic mode [4], that is at constant settings in the matching quadrupoles of IR1 and IR5, and by acting on IR8 and IR2, and on IR4 and IR6, in order to modify β^* at IP1 and IP5, respectively.
The choice of the (constant) matching quadrupole settings in IR1 and IR5 during β^*-levelling corresponds to a constant pre-squeezed β^*, namely $\beta^*_{\rm Pre}$, while the dynamic variations in SB of the IR2, IR4, IR6 and IR8 quadrupole settings modify the actual of β^* value at IP1 and IP5, as follows:

$$\beta^* \equiv \beta^*_{\rm Pre}/r_{\rm Tele}\,, \tag{1}$$

where $r_{\rm Tele}$ is an optics parameter referred to as the so-called telescopic index. The telescopic index, or its inverse $1/r_{\rm Tele}$, also corresponds to the relative increase of the peak β-function induced by this gymnastics in the four arcs adjacent to IR1 and IR5. In order to minimise this optics perturbation during the telescopic β^*-levelling beam process, the initial collision optics (at start of stable beam) shall be anti-telescopic ($r_{\rm Tele} \leq 1$), while the final collision optics shall be telescopic ($r_{\rm Tele} \geq 1$). Furthermore, the pre-squeezed β^* shall be chosen as the geometric mean of the initial and final β^* values, namely:

$$\beta^*_{\rm Pre} = \sqrt{\beta^*_{\rm start} \times \beta^*_{\rm end}} = 60\,{\rm cm\ for\ 2023/2024.} \tag{2}$$

In order to maximize the synergy in terms of optics between 2022 and 2023/2024, the same pre-squeezed β^* will be chosen for 2022. In order words, the β^*-levelling range in 2022, from 60 cm down to 30 cm will correspond to a telescopic index range from 1 to 2 (compared to 40/25=1.6 at 25 cm in 2018 [29]), while the β^*-range in 2023/2024, from 1.2 m down to 30 cm, will be achieved by a change of the telescopic index from 0.5 to 2 in stable beam.

2.3 Alice

The collision optics parameters for Alice will not change with respect to Run 2, namely keeping $\beta^* = 10$ m with an external vertical half-crossing angle of 200 μrad at IP2, which is deemed to be acceptable for halo collision at an instantaneous luminosity of $6 \times 10^{30}\,{\rm cm^{-2}s^{-1}}$ [37] (compared to $2.5 \times 10^{30}\,{\rm cm^{-2}s^{-1}}$ in Run 2).

2.4 LHCb

The LHCb luminosity was stably levelled at $4 \times 10^{32}\,{\rm cm^{-2}s^{-1}}$ throughout the whole of Run 2 and a good fraction of Run 1, using the parallel separation at IP8. Following the LHCb upgrade phase I which took place in LS2 [38], the LHCb luminosity is planned to be levelled at $2 \times 10^{33}\,{\rm cm^{-2}s^{-1}}$ for the production years 2023-2024, but at a somewhat lower value in 2022, which is considered as a commissioning year for the upgraded detector. Taking into account the above performance ramp up schedule, together with the request that the levelling time at LHCb should be similar or larger than the optimal fill length for ATLAS and CMS, namely

$$\mathcal{R} \equiv \frac{T^{\rm (LHCb)}_{\rm LeV}}{T^{\rm (ATLAS,CMS)}_{\rm Opt}} \gtrsim 1\,, \tag{3}$$

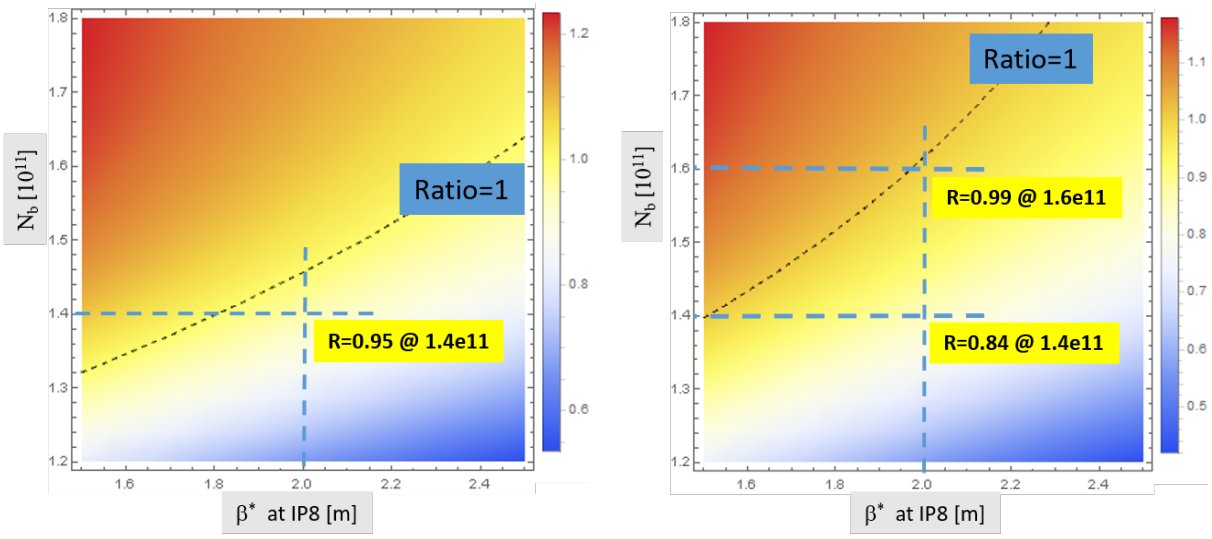

(a) 2022 (b) 2023/2024

Figure 8: Ratio between LHCb levelling time and optimal fill length for ATLAS and CMS as a function of β^* at IP8 and of the bunch population at start of stable beam. The LHCb luminosity is assumed to be levelled at $1.5 \times 10^{33}\,\mathrm{cm}^{-2}\mathrm{s}^{-1}$ in 2022 (left picture), and set to its Run 3 target value of $2.0 \times 10^{33}\,\mathrm{cm}^{-2}\mathrm{s}^{-1}$ in 2023/2024. The beam energy is 6.8 TeV. The assumptions made on the other parameters can be found in the text.

a collision β^* of 2 m at IP8 seems to be an appropriate choice over the whole of Run 3 (to be compared with $\beta^* = 10$ m in 2015/2016, and then $\beta^* = 3$ m later in 2017/2018). Indeed, in order to justify this choice, a color plot of the $\mathcal{R}$ ratio is shown in Fig. 8, as a function of β^* and of the bunch population at start of stable beam, assuming an emittance of $\gamma\epsilon = 2.5\,\mu$m at the end of fill, 2736 and 2376 collisions at IP1/5 and IP8 (see Tab. 2), respectively, a turn around time of 5.0 h, and an effective cross section of 110 mb[1]. For 2022 (commissioning year for the new detector) shown in Fig. 8(a), this ratio has been calculated assuming a levelled luminosity of $1.5 \times 10^{33}\,\mathrm{cm}^{-2}\mathrm{s}^{-1}$, and a horizontal external half-crossing angle of $200\,\mu$rad, corresponding to an internal half crossing-angle of $339\,\mu$rad at 6.8 TeV for the worst polarity of the LHCb spectrometer. For 2023/2024 [see Fig. 8(b)], the levelled luminosity is set to its target value of $2.0 \times 10^{33}\,\mathrm{cm}^{-2}\mathrm{s}^{-1}$, and the external half-crossing angle of $200\,\mu$rad is assumed to be deployed in the vertical plane (see later), corresponding to an internal (tilted) angle of about $250\,\mu$rad (more precisely $243.5\,\mu$rad at 6.8 TeV), regardless of the polarity of the LHCb spectrometer. As illustrated in Fig. 8 for $\beta^* = 2$ m at IP8, the $\mathcal{R}$ ratio is expected to be very close to 1 in 2022 ($\mathcal{R} = 0.95$ for $N = 1.4 \times 10^{11}$ p/b and a levelled luminosity of $1.5 \times 10^{33}\,\mathrm{cm}^{-2}\mathrm{s}^{-1}$), and should comfortably exceed 1 in 2023/2024 (for $N = 1.8 \times 10^{11}$ p/b) at the target luminosity of $2.0 \times 10^{33}\,\mathrm{cm}^{-2}\mathrm{s}^{-1}$.
A second demand from the LHCb experiment in Run 3 is to keep similar physics conditions at the IP, regardless of the spectrometer polarity. When the external crossing angle is horizontal, typically in the range of $\Theta_c/2 = -200\,\mu$rad (for Beam 1), the internal half-crossing angle indeed drastically

[1]For the sake of robustness study, in the present purpose, a turn around time of 5.0 h and an effective cross section of 110 mb were chosen, because they lead to slightly worse predictions for the $\mathcal{R}$ factor compared to the ones that would be obtained by taking the values of 4.5 h and 100 mb which were used to estimate the ATLAS and CMS performance in Tab. 3.

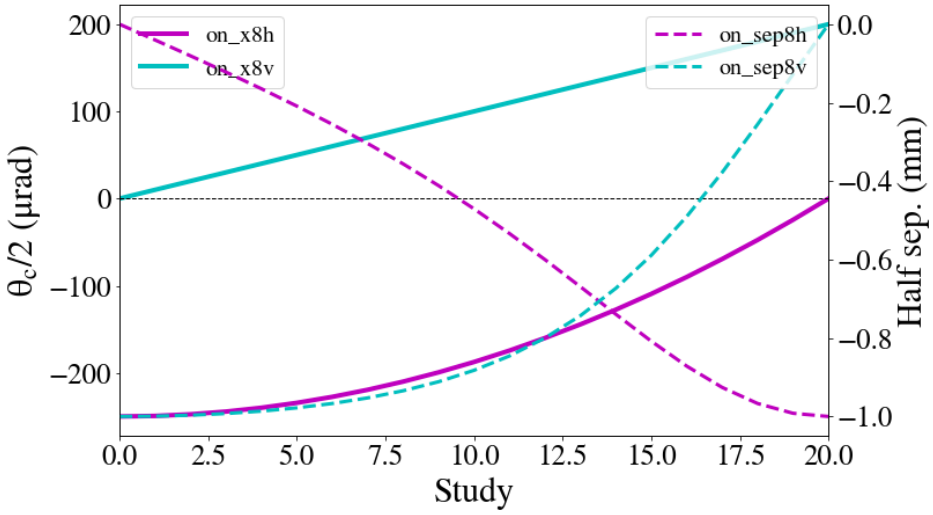

Figure 9: Evolution of the crossing knobs at IP8 to rotate the external crossing angle from the horizontal to the vertical plane. This beam process is planned to be implemented in 2023/2024 at the end of the ramp, just before the squeeze.

changes by $\pm 139\,\mu$rad (at 6.8 TeV) depending on the polarity of the spectrometer. In this respect a vertical external crossing angle will be implemented in Run 3, using a dedicated rotation beam process recently designed, which is independent from the LHCb spectrometer polarity, and will be inserted at the EoR, just before the squeeze. The evolution of the crossing bump knobs during this beam process is shown in Fig. 9, where the EoR internal crossing angle passes from the horizontal plane to a skewed plane [$\left(p_x^*, p_y^*\right) = (-200 \pm 139\,\mu\text{rad},\ 0) \rightarrow (\pm 139\,\mu\text{rad},\ 200\,\mu\text{rad})$ for Beam 1], and the parallel separation, initially in the vertical plane, becomes horizontal at the IP at the end of the beam process. The crossing knob functions during this process are optimized in order to maximize the radial beam-beam separation at the BBLR encounters (with a target of $20\,\sigma$ for the worst separation for either polarity of the LHCb spectrometer). Although this gymnastics is found to be transparent for the dynamic aperture (see later in Sub-Section 3.3), such a beam manipulation has never been run so far at high intensity. Hence, it will only be implemented in 2023/2024 after having been demonstrated in 2022 in a dedicated machine study program. In the presence of e-cloud, the main concern is indeed a possible lifetime dip during the rotation, when the beams cross at 45° the high electron-density lines facing the magnetic poles of the inner triplet quadrupoles.

2.5 Summary

The main collision optics parameters discussed above are summarized in Tab. 5, but keeping in mind all the uncertainties still existing on the beam parameters for Run 3, in terms of management (e.g. heat-load from electron cloud) and preservation (e.g. emittance in the ramp) in the LHC, which may impact the final choice.

Optics Parameters	2022	2023/2024
ATLAS and CMS		
β^* [m] at the start of collision	0.60	1.20
β^* [m] at the end of levelling	0.30	0.30
Pre-squeezed β^* [m]	0.60	0.60
Telescopic index variations in SB	$1.0 \rightarrow 2.0$	$0.5 \rightarrow 2.0$
Half-crossing angle [μrad] (start of collision)	160	160
Half-crossing angle [μrad] (start of β^*-levelling)	145	135
Half-crossing angle [μrad] (end of β^*-levelling)	160	160
Alice		
β^* [m]	10.0	10.0
Half-crossing angle [μrad]	200 (V)	200 (V)
LHCb		
β^* [m]	2.0	2.0
Half-crossing angle [μrad]	200 (H)	200 (V)

Table 5: Main optics parameters in collision for the four LHC experiments in Run 3.

3 Beam physics concerns and LHC hypercycle in Run 3

With the machine configuration defined in collision (see Section 2), and the beam parameter range specified for 2022 and 2023/2024 (see Tab. 2), the LHC hypercycle can be designed and correctly calibrated in order not to limit the machine performance over these two consecutive periods, while taking care of maximizing the synergies in terms of optics evolution over Run 3.

3.1 Injection optics

The 2017/2018 injection optics will be kept over the whole Run 3, in particular with $\beta^* = 11/10/11/10$ m at IP1/2/5/8, and a half crossing angle of $170\,\mu$rad in the four experimental insertions. Indeed, tracking studies performed at injection show that the dynamic aperture remains quite insensitive to the long-range beam-beam effect up to a bunch population of 1.8×10^{11} p/b, even using the pessimistic assumption of a transverse emittance of $2.5\,\mu$m (see Fig. 10). Based on these simulations, the main degradation of the dynamic aperture actually comes from the linear chromaticity and the Landau octupoles (MO), the settings of which are not expected to change at injection with respect to Run 2 (within a possible re-scaling with emittance of the MO current in order to work at constant tune spread [39]).

3.2 Energy ramp

In order to minimise the turn around time, most of the optics manipulations should be performed in the ramp, with the aim to arrive at flat-top energy with an optics configuration which is the one, or very close to the one, targeted for the start of stable beam. In this respect, a so-called combined ramp and squeeze was deployed in Run 2, bringing β^* as low as 1 m at the end of the 2017 and 2018 nominal ramp, compared to $\beta^* = 11$ m at injection and 30 cm at start of stable beam (see e.g.

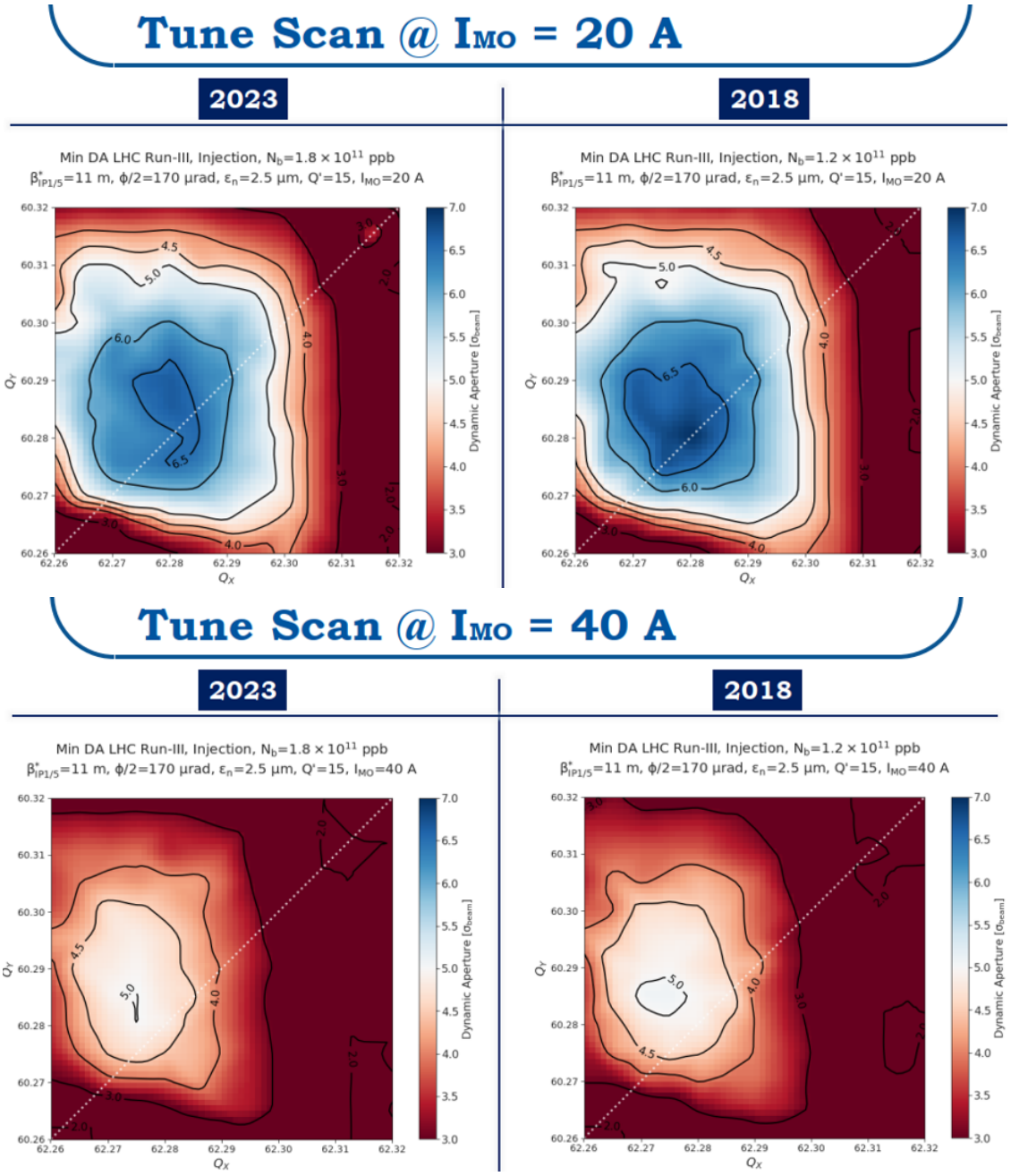

Figure 10: Tune scan at injection using the 2017/2018 LHC injection optics for a bunch population of 1.8×10^{11} p/b (2023) and 1.2×10^{11} p/b (2018), for two possible settings of Landau octupole currents (20 A and 40 A for the top and bottom pictures, respectively), and a linear chromaticity set to $Q' = 15$ units. A transverse normalised emittance of $\gamma\epsilon = 2.5\,\mu$m is assumed in both cases. The long-range beam-beam effects do not seem to have a significant impact on the dynamic aperture at higher bunch intensity.

[29]). With the machine aperture to be revalidated after LS2, such an EoR β^* is however deemed to be too aggressive for 2022. It is therefore proposed to relax the EoR β^* to 2 m for 2022, which offers some synergies with the 2023/2024 optics (see later). This is possible at a marginal cost for the squeeze duration in 2022, which will take place at flat top energy in order to bring β^* down to the prescribed value of 60 cm at start of stable beam (see Tab. 5). For 2023/2024, the idea is then to further push the pre-squeezed β^* down to $\beta^*_{\rm Pre} = 1$ m at the EoR (as in 2017/2018), but also to deploy in parallel the anti-telescopic squeeze, such as to arrive at flat top energy with a tele-index of $r_{\rm Tele} = 0.5$ (corresponding to the telescopic conditions at the start of collisions for 2023/2024, see Tab. 5), i.e. still corresponding $\beta^* \equiv \beta^*_{\rm Pre}/r_{\rm Tele} = 2$ m at the EoR. In addition to the beneficial impact on the turn around time, the combined ramp and telescopic squeeze proposed for 2023/2024 has the advantage of building up some margin in terms of Landau octupole settings for a bunch population of 1.8×10^{11} p/b (see the expected octupole thresholds in Tab. 6).

Scenario	$r_{\rm Tele} = 1.0$	$r_{\rm Tele} = 0.6$	$r_{\rm Tele} = 0.5$	$r_{\rm Tele} = 0.4$
$\gamma\epsilon = 1.8\,\mu$m	550	480	430	360
$\gamma\epsilon = 2.5\,\mu$m	400	350	310	260

Table 6: Expected octupole thresholds [A] at 7 TeV for 1.8×10^{11} p/b for various telescopic index reached at the end of the ramp, for the beam emittance range targeted in Run 3 at flat-top energy, and assuming all MO circuits perfectly working (see [40] for the degradation in case of failure of one or several circuits). The maximum allowed octupole current is 590 A. Run-2-type settings are assumed for the collimators, the new low-impedance collimators installed in LS2 are taken into account in the impedance model, and an empirical factor of 2 is added between strict prediction from the model and expectation, as observed in Run 2 [41]. If the beam energy is not exactly 7.0 TeV at flat-top for Run 3, these thresholds should be re-scaled with $E^{5/2}$.

Ideally, the 2023/2024 ramp should push β^* down to 1.2 m (see Tab. 5), i.e. $\beta^*_{\rm Pre} = 60$ cm at a tele-index of $r_{\rm Tele} = 0.5$, in order to strictly get rid of any optics squeeze period at flat-top energy. On the other hand, the 60 cm pre-squeezed optics is matched with a very low current for the Q6 matching quadrupoles in IR1 and IR5 (~ 200 A at $\beta^*_{\rm Pre} = 60$ cm, vs. ~ 750 A at $\beta^*_{\rm Pre} = 1.0$ m), in order to offer optimal beam conditions to the AFP and PPS forward physics experiments (with a maximized normalized dispersion at the Roman Pots). With the existing uniquadrant power supplies feeding the Q6 magnets, such a reduction of the Q6 current only relies on the natural decay time of the circuit, of the order of 2 minutes. As a result, the ramp would be too short to accommodate this last optics transition, in addition to all the above mentioned optics manipulations, such that a mini-squeeze ($\lesssim 4$ minutes) cannot be avoided for the 2023/2024 period of Run 3.
The timing, energy and optics structure of the 2022 and 2023/2024 ramp (version compatible with 6.5 TeV or beyond) is shown in Tab. 7, with the main features summarized below.

- Both for 2022 and 2023/2024, the optics variation starts at an energy of ~ 1.7 TeV, as for the nominal LHC ramp in 2017/2018.
- The pre-squeeze of the optics down to $\beta^* = 2$ m at IP1, IP5 and IP8 is completed at an energy of ~ 4.5 TeV, while keeping a constant β^* of 10 m at IP2, but reducing the normalised strength of the IR2 triplets to reach a 7-TeV-equivalent-gradient of 205 T/m (vs. 222 T/m for the injection optics, which is needed to correctly adjust the MKI-TDI and MKI-TCLI phase advances and protect the machine against injection failure at 450 GeV).

Energy	Time	Parabolic	2022			2023/2024		
[GeV]	[s]	Fraction	β^* [m] at IP1/2/5/8	r_{Tele}	β^*_{Pre} [m]	β^* [m] at IP1/2/5/8	r_{Tele}	β^*_{Pre} [m]
450.0	0	0.00	11.0/10.0/11.0/10.0	1.00	11.00	11.0/10.0/11.0/10.0	1.00	11.00
452.2	15	0.10	11.0/10.0/11.0/10.0	1.00	11.00	11.0/10.0/11.0/10.0	1.00	11.00
459.0	30	0.10	11.0/10.0/11.0/10.0	1.00	11.00	11.0/10.0/11.0/10.0	1.00	11.00
470.2	45	0.10	11.0/10.0/11.0/10.0	1.00	11.00	11.0/10.0/11.0/10.0	1.00	11.00
486.0	60	0.05	11.0/10.0/11.0/10.0	1.00	11.00	11.0/10.0/11.0/10.0	1.00	11.00
530.9	90	0.05	11.0/10.0/11.0/10.0	1.00	11.00	11.0/10.0/11.0/10.0	1.00	11.00
593.9	120	0.05	11.0/10.0/11.0/10.0	1.00	11.00	11.0/10.0/11.0/10.0	1.00	11.00
705.6	160	0.05	11.0/10.0/11.0/10.0	1.00	11.00	11.0/10.0/11.0/10.0	1.00	11.00
843.5	200	0.05	11.0/10.0/11.0/10.0	1.00	11.00	11.0/10.0/11.0/10.0	1.00	11.00
1054.3	250	0.05	11.0/10.0/11.0/10.0	1.00	11.00	11.0/10.0/11.0/10.0	1.00	11.00
1317.6	300	0.05	11.0/10.0/11.0/10.0	1.00	11.00	11.0/10.0/11.0/10.0	1.00	11.00
1694.0	365	0.05	11.0/10.0/11.0/10.0	1.00	11.00	11.0/10.0/11.0/10.0	1.00	11.00
1896.7	400	0.10	10.0/10.0/10.0/10.0	1.00	10.00	10.0/10.0/10.0/10.0	1.00	10.00
2070.4	430	0.10	9.7/10.0/ 9.7/ 9.7	1.00	9.70	9.7/10.0/ 9.7/ 9.7	1.00	9.70
2244.1	460	0.10	9.3/10.0/ 9.3/ 9.3	1.00	9.30	9.3/10.0/ 9.3/ 9.3	1.00	9.30
2388.9	485	0.14	8.8/10.0/ 8.8/ 8.8	1.00	8.80	8.8/10.0/ 8.8/ 8.8	1.00	8.80
2562.6	515	0.12	8.1/10.0/ 8.1/ 8.1	1.00	8.10	8.1/10.0/ 8.1/ 8.1	1.00	8.10
2753.7	548	0.16	7.0/10.0/ 7.0/ 7.0	1.00	7.00	7.0/10.0/ 7.0/ 7.0	1.00	7.00
2927.4	578	0.10	6.0/10.0/ 6.0/ 6.0	1.00	6.00	6.0/10.0/ 6.0/ 6.0	1.00	6.00
3159.1	618	0.10	5.1/10.0/ 5.1/ 5.1	1.00	5.10	5.1/10.0/ 5.1/ 5.1	1.00	5.10
3419.6	663	0.12	4.4/10.0/ 4.4/ 4.4	1.00	4.40	4.4/10.0/ 4.4/ 4.4	1.00	4.40
3610.7	696	0.14	3.7/10.0/ 3.7/ 3.7	1.00	3.70	3.7/10.0/ 3.7/ 3.7	1.00	3.70
3842.4	736	0.10	3.1/10.0/ 3.1/ 3.1	1.00	3.10	3.1/10.0/ 3.1/ 3.1	1.00	3.10
4195.6	797	0.10	2.5/10.0/ 2.5/ 2.5	1.00	2.50	2.5/10.0/ 2.5/ 2.5	1.00	2.50
4502.5	850	0.14	2.0/10.0/ 2.0/ 2.0	1.00	2.00	2.0/10.0/ 2.0/ 2.0	1.00	2.00
4907.9	920	0.22	2.0/10.0/ 2.0/ 2.0	1.00	2.00	2.0/10.0/ 2.0/ 2.0	0.83	1.66
5197.4	970	0.20	2.0/10.0/ 2.0/ 2.0	1.00	2.00	2.0/10.0/ 2.0/ 2.0	0.73	1.46
5487.0	1020	0.20	2.0/10.0/ 2.0/ 2.0	1.00	2.00	2.0/10.0/ 2.0/ 2.0	0.65	1.30
5950.2	1100	0.20	2.0/10.0/ 2.0/ 2.0	1.00	2.00	2.0/10.0/ 2.0/ 2.0	0.57	1.14
6419.3	1181	0.20	2.0/10.0/ 2.0/ 2.0	1.00	2.00	2.0/10.0/ 2.0/ 2.0	0.50	1.00
6500.0	1210	0.10	2.0/10.0/ 2.0/ 2.0	1.00	2.00	2.0/10.0/ 2.0/ 2.0	0.50	1.00

Table 7: Timing, energy and optics structure of the 2022 and 2023/2024 energy ramp (version compatible with 6.5 TeV or beyond). The first 14 optics are the same for 2022 and 2023/2024. The pre-squeezed β^* of 2 m is reached at 4.5 TeV, above which the ramp continues at constant optics in 2022, while, for the 2023/2024 ramp, an anti-telescope is deployed at constant β^*.

- The ramp then continues at constant optics in 2022, while in 2023/2024 the anti-telescope is deployed at constant β^* to reach a telescopic index of $r_{\mathrm{Tele}} = 0.5$ at the end of the ramp, corresponding to a pre-squeezed β^* of $\beta^*_{\mathrm{Pre}} \equiv r_{\mathrm{Tele}} \times \beta^* = 1$ m at IP1 and IP5.

The 2023/2024 ramp contains a total of 19 different optics, versus 14 and 17 matched points for the two different energy ramps which were used in 2018 for the proton and ion run, respectively. The last five optics of the 2023/2024 ramp are telescopic, and the first 14 can be directly recycled from the 2022 ramp. These two energy ramps have been found to be compatible with the existing ramp and acceleration rate limits of all LHC magnet circuits, within the exception of the present acceleration rate limits of the RQT12 and RQT13 circuits in IR4 and IR6. These limits were indeed specified to rather low values for historical reasons, and will be more than doubled at the end of the 2021 hardware commissioning campaign, namely: from 0.1 A/s^2 up to 0.25 A/s^2, i.e. still much less than the value of 1 A/s^2 which is specified for the same circuits in the four experimental insertions of the LHC.
As soon as the optics is changing (as of 1.7 TeV and beyond), the main challenge is to maintain the normalised aperture of the triplet as large as possible during the ramp. Keeping in mind that the telescopic squeeze can only be deployed when the pre-squeezed β^* is of the order of 2 m or below (when appropriate left and right betatron phase advances can be matched in IR1 and IR5 [4]), and that sufficient time should be left for the telescopic gymnastics in the remaining part of the ramp in order to reach a tele-index of 0.5 on arrival at flat-top, the 2 m pre-squeezed optics shall be placed at an energy of 4.5 TeV (or slightly beyond for a ramp compatibility with 6.8 TeV instead of 6.5 TeV at flat-top energy). At this energy, the normalised triplet aperture is minimal, but is shown to be still be quite comfortable of the order of $16\,\sigma$ (see Fig. 11).

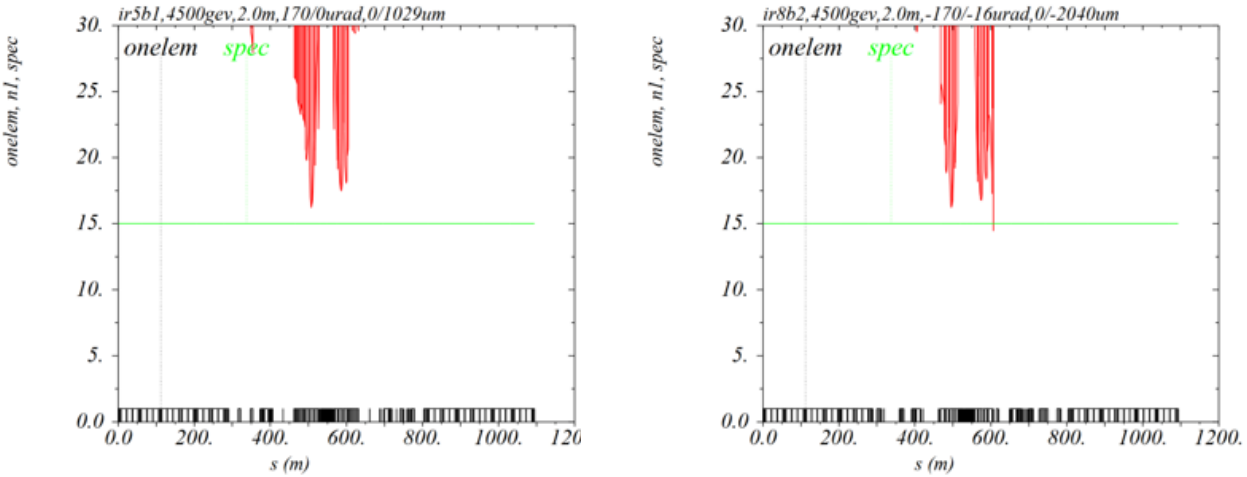

IR5 (Beam 1) IR8 (Beam 2)

Figure 11: Normalised triplet aperture [σ] in IR1/5 (left) and IR8 (right) at a beam energy 4.5 TeV, with $\beta^* = 2.0$ m and a half-crossing angle of 170 μrad, and for a reference normalised emittance of $\gamma\epsilon = 3.5$ μm. The tolerance budget for the closed orbit, β-beating, normalised spurious dispersion and momentum error is assumed to be 2 mm, 21 %, 14 % and 0.86×10^{-3}, respectively (taking the value specified in Tab.4 of [42], but with a doubled budget for the β-beating). The only slight aperture restriction is found in IR8, for Beam 2 only, in the horizontal plane at the TCDDM (D1 mask): $0.5\,\sigma$ are missing with respect to a target of $15\,\sigma$, which is deemed to be acceptable.

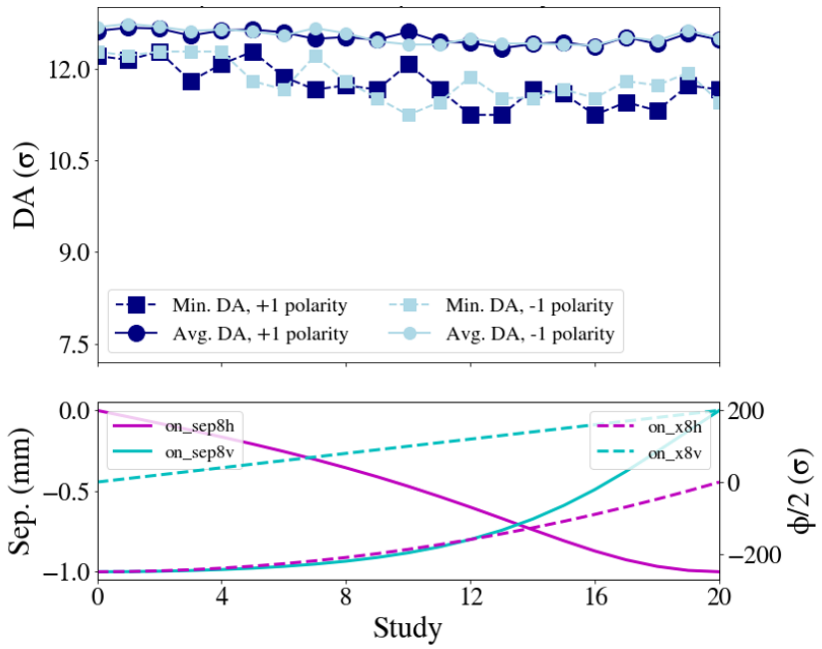

Figure 12: Minimum and average DA (over phase space angle) during the rotation of the external crossing angle in IR8, for both possible polarities of the LHCb spectrometer. This beam process is run EoR with the injection tune [$(Q_{x,y} = (0.270,\ 0.295)$]. The beam energy was set to 7.0 TeV for these simulations, assuming a bunch population of 1.8×10^{11} p/b within an emittance of $\gamma\epsilon = 2.5\,\mu$m (worst case compared to $\gamma\epsilon = 1.8\,\mu$m).

3.3 Crossing angle rotation in LHCb

As discussed in Sub-section 2.4, following dedicated machine studies performed in 2022, a special beam process will be placed right after the end of the ramp in order to rotate the external crossing angle in IR8, from horizontal ($p_x^* = -200\,\mu$rad at the EoR for Beam 1) to vertical with $p_y^* = 200\,\mu$rad EoR for Beam 1 (see Tab. 5 for 2023/2024). This gymnastics is found to be transparent for the dynamic aperture for both polarities of the LHCb spectrometer (see Fig. 12).

3.4 Squeeze

As in Run 2, an optics squeeze beam process will follow, at constant telescopic index, and still using the injection tunes [$(Q_{x,y} = (0.270,\ 0.295)$], namely:

- from $\beta^* = 2$ m down to $\beta^* = 60$ cm at $r_{\text{Tele}} \equiv 1$ in 2022,
- and from $\beta^* = 2$ m down to $\beta^* = 1.2$ m at $r_{\text{Tele}} \equiv 0.5$ in 2023/2024, i.e. $\beta^*_{\text{Pre}} = 1\,\text{m} \rightarrow 60\,\text{cm}$.

The squeeze duration is estimated to be about 4 minutes in 2023/2024 (“mini-squeeze”), limited by the decay time of the Q6 current in IR1 and IR5 (see also the discussion in Sub-section 3.2), with only one intermediate matched point found to be needed (at $\beta^* = 1.56$ m), in order to limit the peak $beta$-beating during optics transition to the percent level.

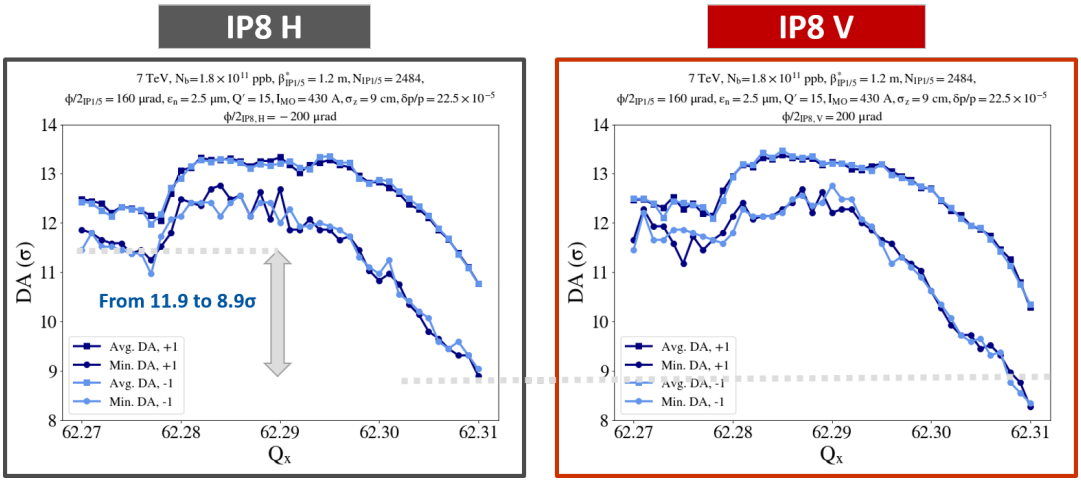

Figure 13: Minimum and average DA (over phase space angle) during the Q-change beam process, for both possible polarities of the LHCb spectrometer, and both possible configurations of the external crossing angle (H or V). This beam process is run after the squeeze to move the working point from the injection tunes [$Q_{x,y} = (0.270,\ 0.295)$] to the collision tunes [$Q_{x,y} = (0.310,\ 0.320)$]. The beam energy was set to 7.0 TeV for these simulations, assuming a bunch population of 1.8×10^{11} p/b within an emittance of $\gamma\epsilon = 2.5\,\mu$m (worst case compared to $\gamma\epsilon = 1.8\,\mu$m).

3.5 Tune change

The so-called "Q-change", which brings the working point onto the collision tune (.31/.32), is conducted after the squeeze, just before putting the beam into collision. This strategy was actually systematically followed during the ATS optics machine development program (as it also offered more margin for linear coupling), but represents a change with respect to Run 2, where this beam process was actually played right after the energy ramp. Indeed, in the absence of head-on beam-beam tune shift, the collision working point was found to be far from optimal for the dynamic aperture in Run 3 (see Fig. 13).

3.6 Adjust

The parallel separation is then completely collapsed to establish head-on collision at IP1 and IP5, and tuned for a given prescribed levelled luminosity at IP2 and IP8. This so-called adjust beam process should last about 60 seconds in Run 3, i.e. twice less than in Run 2, assuming that no or only a small residual IP shift will be requested by the Alice and CMS experiments (compared to -2 mm in 2017/2018), thanks to the Alice detector and LSS5 realignment campaigns which took place in LS2. This beam process is combined with an additional fine tuning of the working point which depends on the actual crossing bump configuration in IR8 and, to a marginal extent, on the transverse beam emittance at flat-top energy. At the end of this beam process, and as illustrated in Fig. 14, the dynamic aperture is still well above $6\,\sigma$ in the case of a horizontal external crossing angle at IP8 [taking $Q_{x,y} = (.316/.321)$ as the best working point at start of stable beam in this case], while the $6.0\,\sigma$ target is just met in the case of a vertical crossing angle [choosing $Q_{x,y} = (.313/.318)$ for this configuration]. The degradation of dynamic aperture in the second case is actually not inherent to this configuration, but comes from the fact that the best working

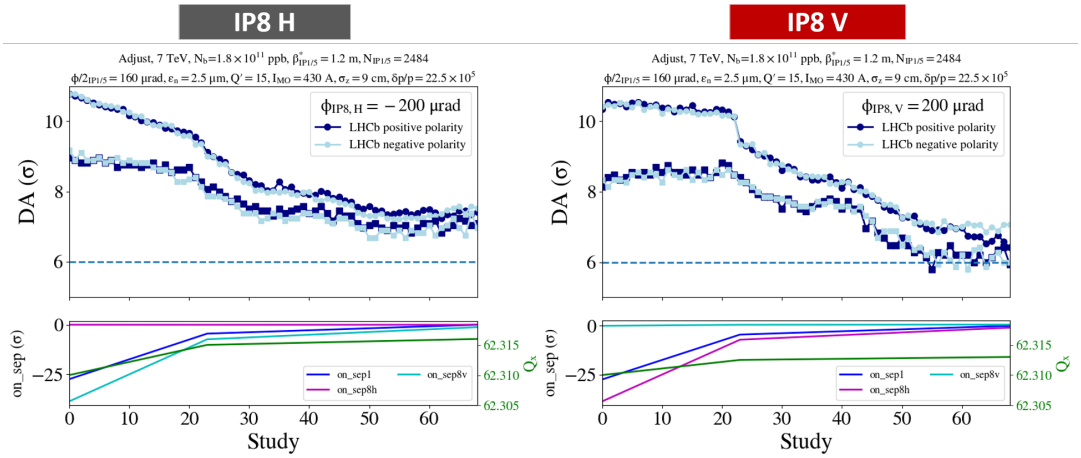

Figure 14: Minimum and average dynamic DA (over phase space angle) during the adjust beam process, where fully head-on collisions are established at IP1 and IP5, while the parallel separation at IP8 and IP2 is tuned for a levelled luminosity of $2 \times 10^{33}\,\mathrm{cm}^{-2}\,\mathrm{s}^{-1}$ for LHCb, and to less than $6 \times 10^{30}\,\mathrm{cm}^{-2}\,\mathrm{s}^{-1}$ for Alice. Both possible polarities of the LHCb spectrometer, and both possible configurations for the external crossing angle in IR8 (H or V) have been looked at. This beam process is run after the Q-change, and combined with an additional fine-tuning of the working point, depending on the actual configuration of the crossing bumps in IR8 and, marginally, on the beam emittance (see details in the text). The beam energy was set to 7.0 TeV for these simulations, assuming a bunch population of 1.8×10^{11} p/b within an emittance of $\gamma\epsilon = 2.5\,\mu$m.

point is shifted closer to the diagonal when the external crossing angle is vertical in IR8 (see Fig. 15). However, assuming less DA degradation in this case is something that would be too risky at this stage, pending the demonstration of a very good control of the linear coupling, which is an on-going effort in the LHC [43].

3.7 Luminosity levelling

The strategy for luminosity levelling at IP1 and IP5 has been described in Sub-section 2.1, namely: first the crossing angle is reduced at constant β^* until reaching the BBLR limit (see Fig. 5), then β^* is decreased, with the crossing angle following the BBLR limit, until reaching the triplet aperture limit ($\beta^* = 30 \rightarrow 28$ cm at $7 \rightarrow 6.5$ TeV). Due to the large variations of the head-on beam-beam tune shift during β^*-levelling (up to $\Delta Q_{\mathrm{bb}} \sim 0.02$), coming from the proton burn-off, the emittance blow up, and from the bunch length and optics parameter changes in SB (see Fig. 6), the working point shall also be varied with β^* (see details on Fig. 16).
As shown in Fig. 16 at the end of luminosity levelling (EoL), i.e. for $\beta^* = 30$ cm, the dynamic aperture is in the range of $5 - 5.5\,\sigma$, basically corresponding to the Run 2 situation in terms of beam and optics parameters at start of stable beam, for which the machine is known to be well-behaved. At start of levelling, the $6\,\sigma$ target is then fully or nearly met (depending on the crossing bump configuration at LHCb). As for the previous beam processes, all the simulations were done keeping quite a lot of margin in terms settings for the linear chromaticity ($Q' = 15$) and octupole settings (430 A, see Tab. 6).

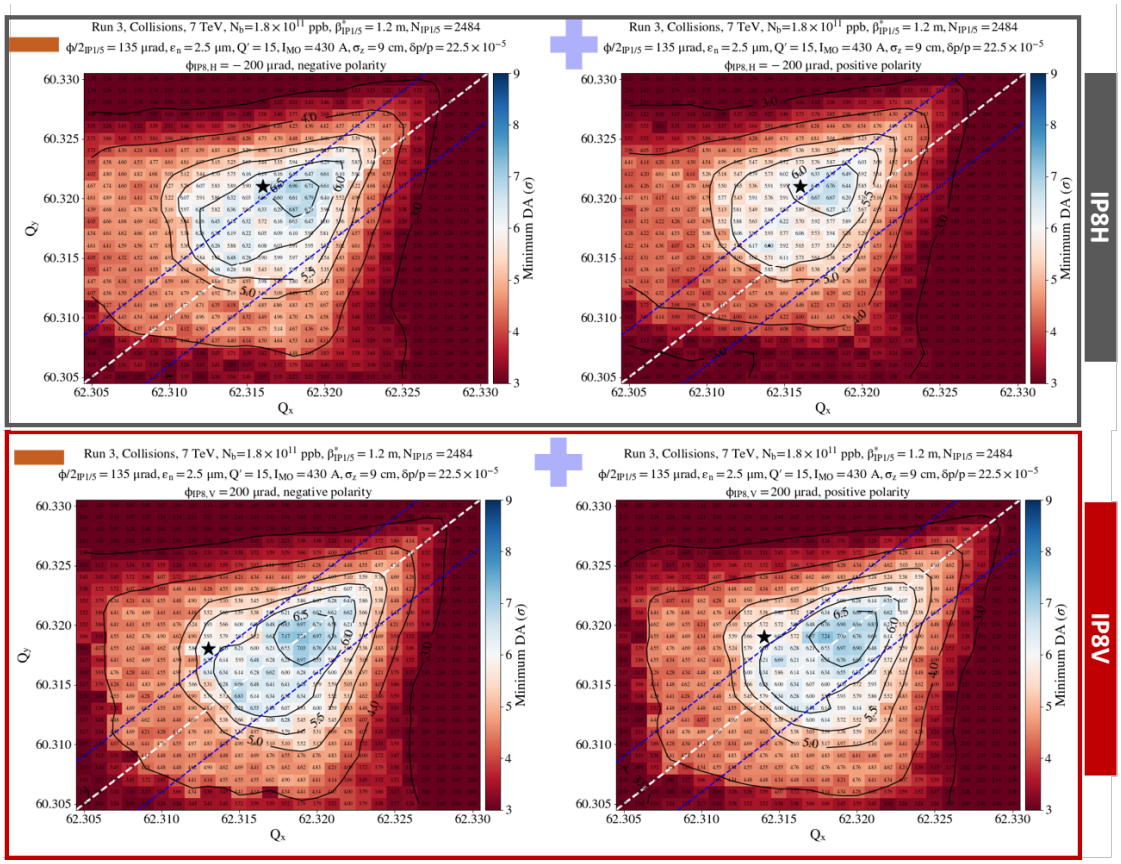

Figure 15: Tune scan (i.e. dynamic aperture versus working point) in collision assuming a horizontal (top) or a vertical (bottom) external crossing angle in IR8, with negative (left) or positive (right) polarity for the LHCb spectrometer. The beam energy was set to 7.0 TeV for these simulations, assuming a bunch population of 1.8×10^{11} p/b within an emittance of $\gamma\epsilon = 2.5\,\mu$m. The other parameters are specified on the top of each picture. On each picture, the dotted lines indicate a fractional tune split of ± 0.004 ($Q_y = Q_x \pm 0.004$), and the star symbols correspond to the best working point for the dynamic aperture while imposing a distance of at least 0.005 with respect to the diagonal (where the control of the linear coupling might become challenging). For a vertical external crossing angle, the best DA island is pushed onto the diagonal compared to the other configuration.

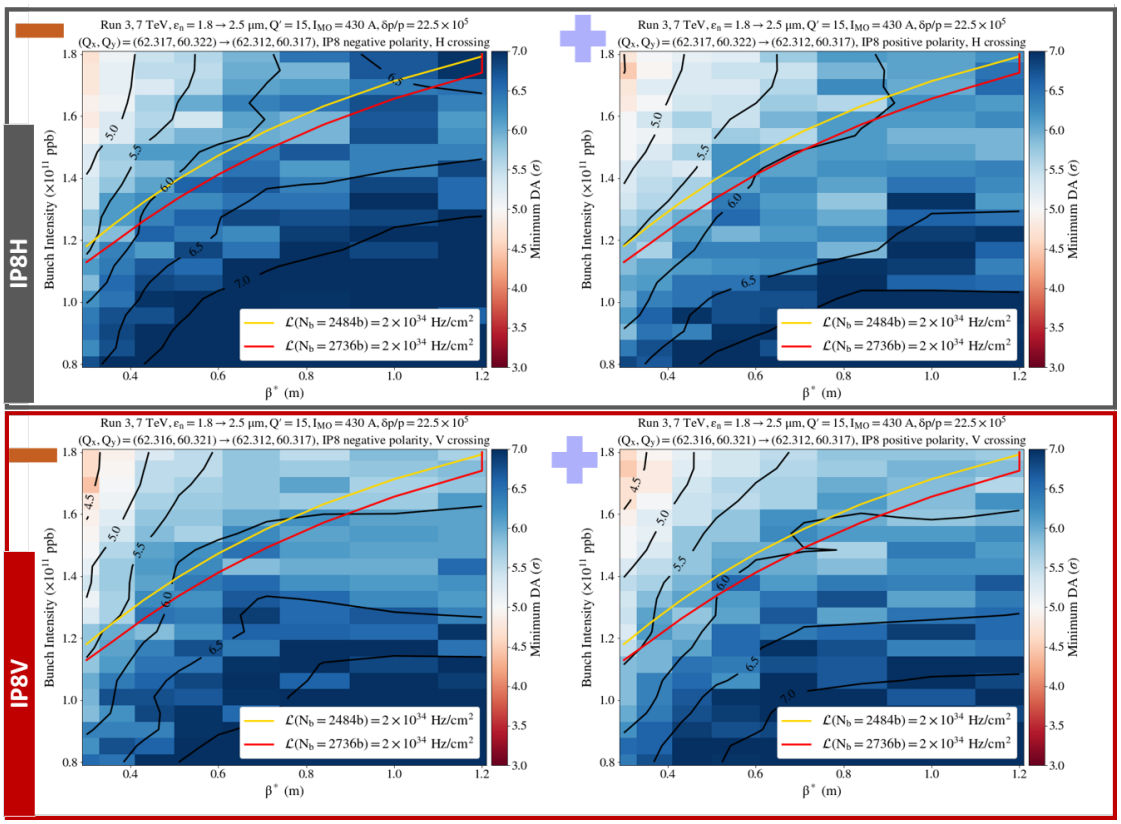

Figure 16: Dynamic aperture as a function of β^* (with the crossing-angle adjusted to the BBLR limit defined in Fig. 5) and of the bunch population, assuming a horizontal (top) or a vertical (bottom) external crossing angle in IR8, with negative (left) or positive (right) polarity of the LHCb spectrometer. The yellow and red contour lines indicate the evolution of the bunch population with β^*, assuming 2484 and 2736 bunches (see Tab. 2), respectively, when levelling at the prescribed luminosity of $2 \times 10^{34}\,\mathrm{cm}^{-2}\,\mathrm{s}^{-1}$ at IP1 and IP5. The beam energy was set to 7.0 TeV for these simulations, with an emittance varying from $\gamma\epsilon = 1.8\,\mu$m at start of levelling ($\beta^* = 1.2$ m), up to $\gamma\epsilon \sim 2.5\,\mu$m at the end of levelling ($\beta^* = 30$ cm) (see 2023/2024 model in Fig. 6). The best working points determined by tracking at the start and end of levelling (and slightly depending on the LHCb configuration at start of levelling) are interpolated linearly at intermediate β^* keeping a distance of 0.005 with respect to the diagonal (see the details on the top of each picture).

3.8 Summary

The sequence of beam processes from injection to collision is summarized in Fig 17, both for 2022 and 2023/2024. The latest versions of the corresponding LHC optics can be found in [44] and [45], for the 2022 and 2023/2024 proton runs, respectively.

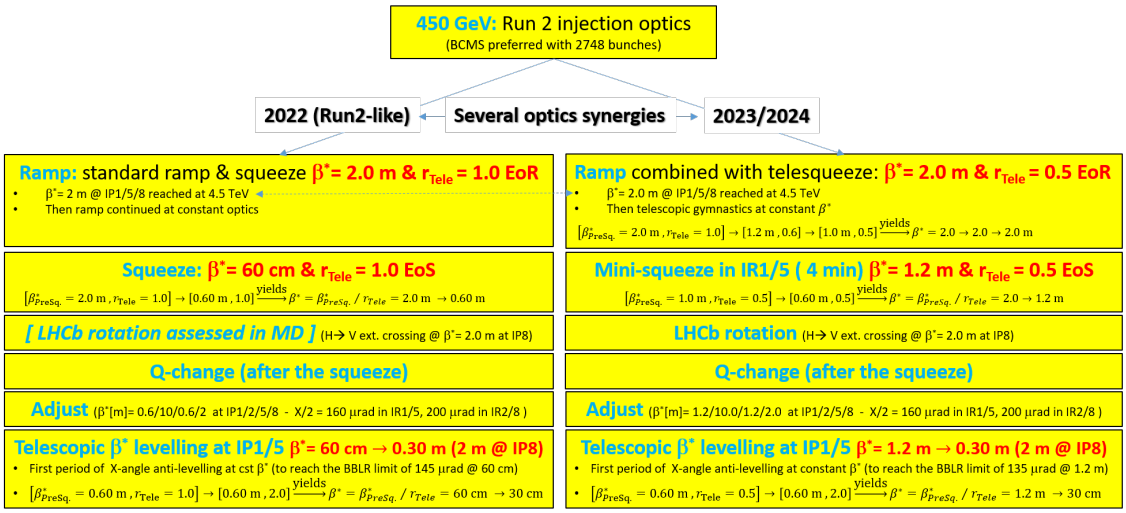

Figure 17: Template for the LHC hypercycle in Run 3, for 2022 (left) and 2023/2024 (right).

4 Summary and Outlook

The completion of the LIU project, one full run in advance with respect to the installation of the HL-LHC, offers a great opportunity to the LHC, both in order to gain experience with high intensity beams, but also to double the luminosity integrated so far by the ATLAS and CMS experiments, while continuing to maximize the beam conditions delivered to the other experiments, including the forward physics experiments. In this context, a beam intensity target of 1.8×10^{11} p/b for the 2023 and 2024 pp runs (and 1.4×10^{11} p/b for 2022) seems to be appropriate, being of course challenging, but a priori not out of reach, for the existing equipment of the LHC ring which are not planned to be upgraded in Run 3. With this target in mind, the machine configuration can be established and correctly calibrated in order not to be a limitation to the machine performance over the full Run 3. The main ingredients and novelties are

- the full deployment of luminosity levelling with β^* for the ATLAS and CMS experiments, operating at the triplet cryo-cooling capacity limit ($L \sim 2.0 \times 10^{34}\,\mathrm{cm}^{-2}\mathrm{s}^{-1}$),
- the exclusive usage of telescopic optics squeezing techniques to vary β^* at IP1 and IP5 (together with the crossing angle in option), over a quite large dynamic range (within a factor of 2 in 2022, and up to a factor of 4 in 2023/2024),
- the deployment of anti-telescopic optics in the ramp as of 2023,

- a careful crossing angle management in IR1 and IR5 in order to maximize the triplet luminosity lifetime, with a total radiation dose deposited in the triplet which is expected in the range of $\sim$ 25 MGy after $\sim$ 400 fb^{-1}, and which, from this point of view, should a priori not prevent a one year extension of Run 3 [33],

- dedicated crossing angle gymnastics in in IR8 (as of 2023), implemented right after the ramp, in order to rotate the external crossing angle from horizontal to vertical, as requested by the LHCb experiment.

Some uncertainties however still remain on the LHC side concerning the compatibility of the 1.8×10^{11} p/b target with the existing beam dump of the LHC, with news expected at the beginning of 2022 (see Sub-Section 1.2.3). Check-points on the injector side, such as the IEF (Injector and Experimental Facility) Workshop planned for December 2021, or the SPS re-commissioning in 2022, might also imply the need to re-optimize the plan (for instance, in case of severe intensity limitations at SPS extraction in 2022, by moving the β^*-levelling beam process either partially or entirely into the squeeze).
Some challenges are also ahead in order to safely and reliably deploy these techniques in operation at high intensity, in particular the new combined ramp and telescopic squeeze foreseen for 2023/2024 (which will deserve dedicated machine studies in 2022), and the above-mentioned telescopic β^*-levelling over a β^*-range of 2 to 4. In this respect, first studies on the optics commissioning strategy already showed that a priori only two collision optics will necessitate an accurate correction in 2022 (at $\beta^* = 60$ cm and 30 cm) for a good control of the β-beating for intermediate optics, and to keep the possible luminosity unbalance between ATLAS and CMS to the percent level during the β^*-levelling process [46]. Experience gained in 2022 will of course be crucial to fine-tune this estimate for the larger β^*-range expected as of 2023, and, in general and if needed, to re-calibrate the overall plan for the rest of Run 3.

Acknowledgements

R. Jones is warmly acknowledged for his accurate and patient work of proofreading and commenting on the draft manuscript of this report.

References

[1] O. Brüning, P. Collier, P. Lebrun, S. Myers, R. Ostojic, J. Pool and P. Proudlock (Ed.), "LHC Design Report, v.1 : the LHC Main Ring", *CERN-2004-003-V-1*, CERN, Geneva, Switzerland, https://cds.cern.ch/record/782076, 2004.

[2] H. Damerau et al., "LHC Injectors Upgrade: Technical Design Report", *CERN-ACC-2014-0337*, 2014.

[3] O. Aberle et al., "High-Luminosity Large Hadron Collider (HL-LHC): Technical design report", *CERN-2020-010*, CERN, Geneva, Switzerland, https://cds.cern.ch/record/2749422, 2020.

[4] S. Fartoukh, “Achromatic Telescopic Squeezing scheme and its Application to the LHC and its Luminosity Upgrade”, *Phys. Rev. ST Accel. Beams , Vol. 16, 111002*, 2013.

[5] H. Damerau et al., “RF manipulations for higher beam brightness LHC-type beams”, *CERN-ACC-2013-0210*, 2013.

[6] H. Damerau et al., “LIU: Exploring alternative ideas”, In proceedings of the Review of LHC and Injector Upgrade Plans Workshop, https://indico.cern.ch/event/260492/, 2018.

[7] G. Rumolo, H. Bartosik, V. Kain and M. Meddahi, “What to expect from the injector during Run 3”, in Proc. 9th LHC Operations Evian Workshop, Evian, France, 30-1 January-February 2019, *CERN-ACC-2019-059*, 2019.

[8] F. M. Velotti et al., “LHC injection system along run II”, in Proc. 9th LHC Operations Evian Workshop, Evian, France, 30-1 January-February 2019, *CERN-ACC-2019-059*, 2019.

[9] R. Bruce, “Machine Configuration Options (and Limits)”, presented at the Chamonix LHC Performance Workshop 2018, 29 January - 2 February 2018, Chamonix, France, https://indico.cern.ch/event/676124, 2018.

[10] F. Carra et al., ”Damage Thresholds for New Collimator Materials, Experiment Detectors and SC Magnet Components”, Presented at the 2019 MPP Workshop, 7-8 May 2019, Chateau de Bossey, Switzerland, https://indico.cern.ch/event/803870/, 2019.

[11] C. Bracco et al., “LBDS Performance in Run II”, in Proc. 9th LHC Operations Evian Workshop, Evian, France, 30-1 January-February 2019, CERN Accelerator Report *CERN-ACC-2019-059*, 2019.

[12] V. Rizzoglio, A. Lechner, et al., “Energy deposition on the dump block and other associated parameters”, Presented at the LHC beam dump block review on LS2 upgrades for Run3 operation, 16 January 2020, https://indico.cern.ch/event/861851/, 2020.

[13] J. Maestre Heredia, et al., “LHC External Beam Dumps (TDE) Modifications and upgrades during LS2 for Run3 ”, *LHC-TDE-EN-0001*, https://edms.cern.ch/document/2437709, 2021.

[14] A. Perillo-Marcone et al., “LHC Dump Assembly: Operational Feedback and Future Prospective”, in Proc. 9th LHC Operations Evian Workshop, Evian, France, 30-1 January-February 2019, CERN-ACC-2019-059, 2019.

[15] V. Kuksenko et al., ”Investigation of SIGRAFLEX samples exposed in the HiRadMat facility (CCFE study)”, CERN internal report (15 May 2020) available at https://edms.cern.ch/document/2380563, 2020.

[16] B. Goddard, L. Massidda, A. Presland, W. Weterings, “Dynamic Stresses in the LHC TCDS Diluter from 7 TeV Beam Loading”, Proc. 10th European Particle Accelerator Conference, Edinburgh, UK, 26 - 30 Jun 2006, p. 1511-1513, 2006.

[17] F.X. Nuiry, et al., "TCDS/TCDQ for Run III and HL-LHC: Summary of the ongoing thermo-mechanical calculations", presented at the LHC Beam Dump System Review, CERN, Geneva, Switzerland, 05/02/0219, https://indico.cern.ch/event/784431, 2019.

[18] J. Maestre Heredia, F.X. Nuiry, P. Andreu Munoz, et al., "TCDQ/S simulation results", presented at HL-LHC WP14 Meeting, CERN, Geneva, Switzerland, 30 June 2021, https://indico.cern.ch/event/1055069/, 2021.

[19] C. Bracco, et al., "Beam Based Measurements to Check Integrity of LHC Dump Protection Elements", Proceedings of the 7th International Particle Accelerator Conference, Busan, Korea, 8 - 13 May 2016, THPOR051, p. 3908-3910, 2016.

[20] J. Maestre Heredia, et al., "TCDQ thermo-mechanical analysis for the HL-LHC", presented at the 7th LHC Run-III Configuration Working Group Meeting, CERN, Geneva, Switzerland, 09/11/2018, https://indico.cern.ch/event/762849/, 2018.

[21] C. Bracco, Private Comm., 2018.

[22] H. Timko et al., "LHC Longitudinal Beam Dynamics in Run-II", in Proc. 9th LHC Operations Evian Workshop, Evian, France, 30-1 January-February 2019, *CERN-ACC-2019-059*, 2019.

[23] H. Timko et al., "Estimated LHC RF system performance reach at injection during Run-III and beyond", *CERN-ACC-NOTE-2019-0005*, 2019.

[24] G. Ferlin et al., "Cryogenics experience during Run2 and impact of LS2 on next run", in Proc. 9th LHC Operations Evian Workshop, Evian, France, 30-1 January-February 2019, *CERN-ACC-2019-059*, 2019.

[25] G. Skripka and G. Iadarola, " Beam-induced heat loads on the beam screens of the HL-LHC arcs", *CERN-ACC-NOTE-2019-0041*, 2019.

[26] B. Petersen and C. Schwick, "Experiment requests and constraints for Run 3", in Proc. 9th LHC Operations Evian Workshop, Evian, France, 30-1 January-February 2019, *CERN-ACC-2019-059*, 2019.

[27] S. Papadopoulou, "What do we understand on the emittance growth?", in Proc. 9th LHC Operations Evian Workshop, Evian, France, 30-1 January-February 2019, *CERN-ACC-2019-059*, 2019.

[28] S. Paramesvaran, L. Silvestris, G. Boudoul, "CMS feedback to LPC", LHC Physics Coordination (LPC) Meeting, 20/05/2019, https://indico.cern.ch/event/820221/, 2019.

[29] J. Wenninger, "Operation and Configuration of the LHC in Run 2", CERN Accelerator Notes *CERN-ACC-NOTE-2019-0007*, CERN, 2019.

[30] X. Buffat et al., "Strategy for Landau damping of head-tail instabilities at top energy in the HL-LHC", *CERN-ACC-NOTE-2020-0059*, 2020.

[31] S. Papadopoulou, F. Antoniou, I. Efthymiopoulos, M. Hostettler, G. Iadarola, N. Karastathis, S. Kostoglou, Y. Papaphilippou, "Monitoring and Modelling of the LHC Emittance and Luminosity Evolution in 2018", J. Phys.: Conf. Ser. **1350** 012011, 2019.

[32] M. Albrow et al., CMS and TOTEM Collaborations, "CMS-TOTEM Precision Proton Spectrometer", *TOTEM-TDR-003* and *CMS-TDR-13*, CERN, 2014.

[33] F. Cerutti, "Radiation Estimate to the Triplet and IT Correctors", Presented at the 419th LHC Machine Committee (LMC), 23/06/2021, https://indico.cern.ch/event/1048180, 2021.

[34] S. Fartoukh and S. Kostoglou, "Latest Run 3 optics versions with requested β^* granularity", Presented at the 22th LHC Run-III Configuration Working Group Meeting, CERN, Geneva, Switzerland, 08/10/2021, https://indico.cern.ch/event/1074467/, 2021.

[35] S. Fartoukh, M. Ilaria Besana, Francesco Cerutti, Luigi S. Esposito, "LHC triplet lifetime versus operational scenario in ATLAS and CMS", presented at the 225th LHC Machine Committee, 8 July 2015, https://indico.cern.ch/event/406858, 2015.

[36] R. Staszewski et al., AFP Collaboration, "The AFP Project", *Acta Phys. Pol. B 42, pp. 1615-1624*, 2011.

[37] The Alice Collaboration, "Future high-energy pp programme with ALICE", *CERN-LHCC-2020-018*, http://cds.cern.ch/record/2724925, 2020.

[38] The LHCb Collaboration, "Framework TDR for the LHCb Upgrade : Technical Design Report", *CERN-LHCC-2012-007*, https://cdsweb.cern.ch/record/1443882, 2012.

[39] G. Iadarola, "Electron cloud instabilities at injection", presented at the 14th LHC Run-III Configuration Working Group Meeting, CERN, Geneva, Switzerland, 03/04/2021, https://indico.cern.ch/event/905284/, 2021.

[40] S. Fartoukh, "Impact and possible mitigation measures in case of failure of lattice sextupole and octupole circuits in Run 3", *CERN-ACC-NOTE-2020-0057*, 2020.

[41] X. Buffat et al., "Transverse Instabilities", in Proc. 9th LHC Operations Evian Workshop, Evian, France, 30-1 January-February 2019, CERN Accelerator Report *CERN-ACC-2019-059*, 2019.

[42] R. Bruce et al., "Updated parameters for HL-LHC aperture calculations for proton beams", *CERN-ACC-2017-051*, 2017.

[43] E.-J. Hoydalsvik and T. Persson, "Reaching the sub per mil level coupling corrections in the LHC", Proc. 12th International Particle Accelerator Conference 2021, Campinas, SP, Brazil, May 24-28, 2021.

[44] S. Fartoukh, "Latest version of the LHC Optics for the 2022 pp Run", /afs/cern.ch/eng/lhc/optics/runIII/RunIII_dev/2021_V6/PROTON, 2021.

[45] S. Fartoukh, "Latest version of the LHC Optics for the 2023 and 2024 pp Runs", /afs/cern.ch/eng/lhc/optics/runIII/RunIII_dev/2022_V5/PROTON, 2021.

[46] T. Persson and E.-J. Hoydalsvik, "Linear optics commissioning scenarios", presented at the 21th LHC Run-III Configuration Working Group Meeting, CERN, Geneva, Switzerland, 18/06/2021, https://indico.cern.ch/event/1037633/, 2021.